

Electroweak precision observables and Higgs-boson signal strengths in the Standard Model and beyond: present and future

J. de Blas,^a M. Ciuchini,^b E. Franco,^a S. Mishima,^c M. Pierini,^d L. Reina,^{e,f} and L. Silvestrini^a

^a*INFN, Sezione di Roma,
Piazzale A. Moro 2, I-00185 Rome, Italy*

^b*INFN, Sezione di Roma Tre,
Via della Vasca Navale 84, I-00146 Roma, Italy*

^c*Theory Center, Institute of Particle and Nuclear Studies (IPNS),
High Energy Accelerator Research Organization (KEK), 1-1 Oho, Tsukuba, 305-0801, Japan*

^d*CERN,
Geneva, Switzerland*

^e*Physics Department, Florida State University,
Tallahassee, FL 32306-4350, USA*

^f*Kavli Institute for Theoretical Physics, University of California,
Santa Barbara, CA 93106-4030, USA*

E-mail: jorge.deblasmateo@roma1.infn.it,
marco.ciuchini@roma3.infn.it, enrico.franco@roma1.infn.it,
satoshi.mishima@kek.jp, maurizio.pierini@cern.ch, reina@hep.fsu.edu,
luca.silvestrini@roma1.infn.it

ABSTRACT: We present results from a state-of-the-art fit of electroweak precision observables and Higgs-boson signal-strength measurements performed using 7 and 8 TeV data from the Large Hadron Collider. Based on the `HEPfit` package, our study updates the traditional fit of electroweak precision observables and extends it to include Higgs-boson measurements. As a result we obtain constraints on new physics corrections to both electroweak observables and Higgs-boson couplings. We present the projected accuracy of the fit taking into account the expected sensitivities at future colliders.

1 Introduction

Looking for indirect evidence of physics beyond the Standard Model (SM) has become a strong component of the Large Hadron Collider (LHC) physics program. Run I of the LHC revealed the existence of a Higgs boson (H) with characteristics very similar to the Higgs boson of the SM. Identifying the H particle with the SM Higgs boson fully determines the SM Lagrangian, so that all electroweak precision observables (EWPO) and all Higgs-boson couplings can be predicted within the SM. Thus, EWPO and Higgs-boson observables play a key role in constraining extensions of the SM and in searching for new physics (NP).

In this paper we present a global fit of both EWPO and Higgs-boson signal strengths, based on results obtained at LEP, SLC, the Tevatron, and during Run I of the LHC, at both 7 and 8 TeV center-of-mass energies. The fit is carried out using the `HEPfit` package [1, 2], a general tool to combine direct and indirect constraints on the SM and its extensions. In particular, we use `HEPfit` to perform a statistical analysis of EWPO and Higgs-boson signal-strength measurements in the SM and beyond. Most importantly, we obtain constraints on possible deviations of the Higgs-boson couplings to both gauge bosons and fermions from the SM prediction. Finally, we investigate the impact of the high-luminosity upgrade of the LHC and of future e^+e^- colliders on the precision of the fit in the SM and beyond. Our analysis updates the study of ref. [3] and extends it to include recent Higgs-boson physics results. Results from the initial stages of this project were presented in [4–6] and have by now been updated to reflect all the most recent developments in theoretical calculations and experimental measurements. A model-independent study of NP effects on both EWPO and Higgs-boson couplings based on an effective-field-theory approach will be presented in a forthcoming paper [7].

Recent updates of global fits to EWPO in the SM and beyond, as well as constraints on Higgs-boson couplings, have been presented in refs. [8, 9]. In spite of the different statistical methods and of the different inputs, we obtain compatible results for the EWPO fit. We however consider more NP parameterizations, implement constraints from Higgs-boson signal strengths, and extend the analysis of future accuracies to more scenarios.

The paper is organized as follows. In section 2 we briefly describe the `HEPfit` package. In sections 3 and 4 we summarize results for the electroweak (EW) precision fits of the SM and its extensions, while we illustrate in section 5 the constraints we obtain for non-standard Higgs-boson couplings. The impact of future colliders on our analysis is discussed in section 6. In section 7 we present our conclusions.

2 The `HEPfit` package

The `HEPfit` package¹ is a general tool to combine direct and indirect constraints on the Standard Model and its extensions, available under the GNU General Public License (GPL) [2]. The `HEPfit` code can be extended to include new observables and NP models which

¹Formerly known as `SUSYfit`, the package has now grown to include more physical observables and multiple models.

can be added to the main core as external modules. Exploiting the Markov-Chain Monte-Carlo implementation provided in the Bayesian Analysis Toolkit (BAT) [10], `HEPfit` can be used as a standalone program to perform Bayesian statistical analyses. Alternatively, it can be used in library mode to compute observables in any implemented model, allowing for phenomenological analyses in any statistical framework. The interested reader can find more details on `HEPfit` in refs. [1, 2]. The first application of the `HEPfit` code has been to update the EW precision fit presented in ref. [5], a detailed explanation of which can be found in [3] and references therein.

In this paper we use `HEPfit` to perform a Bayesian statistical analysis of EWPO and Higgs-boson observables in the SM and beyond. The code for the EWPO and Higgs observables has been written from scratch. The EWPO results have been successfully validated against `ZFITTER` [11].

3 Electroweak precision fit in the Standard Model

In this section we update the fit of EWPO presented in refs. [3, 5], where all relevant formulæ and a detailed overview of the literature can be found. With respect to ref. [3], we include the full two-loop fermionic EW corrections to Z partial decay widths computed in ref. [24], and the four-loop approximate QCD corrections to the W mass computed in ref. [25–27] (we use the updated semi-analytical formula given in ref. [28]).

Among the input parameters, G_μ and α are fixed ($G_\mu = 1.1663787 \times 10^{-5} \text{ GeV}^{-2}$, and $\alpha = 1/137.035999139$ [9]), while $\alpha_s(M_Z)$, $\Delta\alpha_{\text{had}}^{(5)}(M_Z)$, M_Z , m_t , and m_H are taken as floating. We use flat priors for all the SM input parameters, and include the information of their experimental measurements in the likelihood. We assume all experimental distributions are Gaussian. Parameters and results for the various EWPO included in the fit are summarized in table 1, where we also give the references from which the measurements have been taken.

With respect to refs. [3, 5], we have updated m_H [15] and we use the top-quark mass as given by the most up-to-date world average [14]. The values of M_Z [13] and $\Delta\alpha_{\text{had}}^{(5)}(M_Z)$ [12] are unchanged. Concerning $\alpha_s(M_Z)$, we notice that the most recent PDG average [9] is sizably different from the previous one due to the different averaging procedure which also results in a substantial increase in the uncertainty on $\alpha_s(M_Z)$ [9].² The new procedure increases the uncertainty on the lattice determination of $\alpha_s(M_Z)$ (which was previously dominating the average) as well as the error on the global average. Oddly, the new error of the PDG lattice average is comparable to the uncertainty of $\alpha_s(M_Z)$ by FLAG [30], although the FLAG error is dominated by an estimate of the uncertainty associated with the truncation of the perturbative series. In the following, we will use the new PDG average (obtained excluding the EW fit determination) $\alpha_s(M_Z) = 0.1179 \pm 0.0012$ as a reference value. However, in view of the impact on the EW fit of the increased error, we also present the results for the SM fit with the previous PDG average $\alpha_s(M_Z) = 0.1185 \pm 0.0005$ to allow the reader to appreciate the effect of the new average. Finally, we have included in

² The shift in the central value has also been determined by the inclusion of the CMS measurement of the $t\bar{t}$ cross section at $\sqrt{s} = 7 \text{ TeV}$ [29].

	Ref.	Measurement	Posterior	Prediction	1D Pull	nD Pull
$\alpha_s(M_Z)$	[9]	0.1179 ± 0.0012	0.1180 ± 0.0011	0.1185 ± 0.0028	-0.2	
$\Delta\alpha_{\text{had}}^{(5)}(M_Z)$	[12]	0.02750 ± 0.00033	0.02747 ± 0.00025	0.02743 ± 0.00038	0.04	
M_Z [GeV]	[13]	91.1875 ± 0.0021	91.1879 ± 0.0020	91.199 ± 0.011	-1.0	
m_t [GeV]	[14]	173.34 ± 0.76	173.61 ± 0.73	176.6 ± 2.5	-1.3	
m_H [GeV]	[15]	125.09 ± 0.24	125.09 ± 0.24	102.8 ± 26.3	0.8	
M_W [GeV]	[16]	80.385 ± 0.015	80.3644 ± 0.0061	80.3604 ± 0.0066	1.5	
Γ_W [GeV]	[17]	2.085 ± 0.042	2.08872 ± 0.00064	2.08873 ± 0.00064	-0.2	
$\sin^2 \theta_{\text{eff}}^{\text{lept}}(Q_{\text{FB}}^{\text{had}})$	[13]	0.2324 ± 0.0012	0.231464 ± 0.000087	0.231435 ± 0.000090	0.8	
$P_\tau^{\text{pol}} = \mathcal{A}_\ell$	[13]	0.1465 ± 0.0033	0.14748 ± 0.00068	0.14752 ± 0.00069	-0.4	
Γ_Z [GeV]	[13]	2.4952 ± 0.0023	2.49420 ± 0.00063	2.49405 ± 0.00068	0.5	
σ_h^0 [nb]	[13]	41.540 ± 0.037	41.4903 ± 0.0058	41.4912 ± 0.0062	1.3	0.7
R_ℓ^0	[13]	20.767 ± 0.025	20.7485 ± 0.0070	20.7472 ± 0.0076	0.8	
$A_{\text{FB}}^{0,\ell}$	[13]	0.0171 ± 0.0010	0.01631 ± 0.00015	0.01628 ± 0.00015	0.8	
\mathcal{A}_ℓ (SLD)	[13]	0.1513 ± 0.0021	0.14748 ± 0.00068	0.14765 ± 0.00076	1.7	
\mathcal{A}_c	[13]	0.670 ± 0.027	0.66810 ± 0.00030	0.66817 ± 0.00033	0.02	
\mathcal{A}_b	[13]	0.923 ± 0.020	0.934650 ± 0.000058	0.934663 ± 0.000064	-0.6	
$A_{\text{FB}}^{0,c}$	[13]	0.0707 ± 0.0035	0.07390 ± 0.00037	0.07399 ± 0.00042	-0.9	1.5
$A_{\text{FB}}^{0,b}$	[13]	0.0992 ± 0.0016	0.10338 ± 0.00048	0.10350 ± 0.00054	-2.6	
R_c^0	[13]	0.1721 ± 0.0030	0.172228 ± 0.000023	0.172229 ± 0.000023	-0.05	
R_b^0	[13]	0.21629 ± 0.00066	0.215790 ± 0.000028	0.215788 ± 0.000028	0.7	
$\sin^2 \theta_{\text{eff}}^{ee}$	[18]	0.23248 ± 0.00052			2.1	
$\sin^2 \theta_{\text{eff}}^{\mu\mu}$	[19]	0.2315 ± 0.0010			0.07	
$\sin^2 \theta_{\text{eff}}^{ee}$	[20]	0.23146 ± 0.00047			0.1	
$\sin^2 \theta_{\text{eff}}^{e,\mu\mu}$	[21]	0.2308 ± 0.0012	0.231464 ± 0.000087	0.231435 ± 0.000090	-0.5	
$\sin^2 \theta_{\text{eff}}^{\mu\mu}$	[22]	0.2287 ± 0.0032			-0.8	
$\sin^2 \theta_{\text{eff}}^{\mu\mu}$	[23]	0.2314 ± 0.0011			-0.1	

Table 1. Experimental measurement, result, prediction, and pull for the five input parameters ($\alpha_s(M_Z)$, $\Delta\alpha_{\text{had}}^{(5)}(M_Z)$, M_Z , m_t , m_H), and for the set of EWPO considered in the SM EW fit. The values in the column *Prediction* are determined without using the corresponding experimental information (see text). Pulls are calculated both as individual pulls (*1D Pull*) and as global pulls (*nD Pull*) for sets of correlated observables (see text), and are given in units of standard deviation. Groups of correlated observables are identified by shades of grey.

the fit the latest determinations of the effective leptonic angle, $\sin^2 \theta_{\text{eff}}^{\text{lept}}$, obtained at the Tevatron and at Run I of the LHC.

For each observable, we give the experimental information used as input (*Measurement*), together with the output of the combined fit (*Posterior*), and the *Prediction* of the same quantity. The latter is obtained from the posterior predictive distribution derived from a combined analysis of all the other quantities. The compatibility of the constraints is then tested computing the *Pull* for each observable as the difference between the corresponding prediction and measurement in units of the combined standard deviation (*1D Pull*). Care must be taken in defining the pull for experimentally correlated observables.

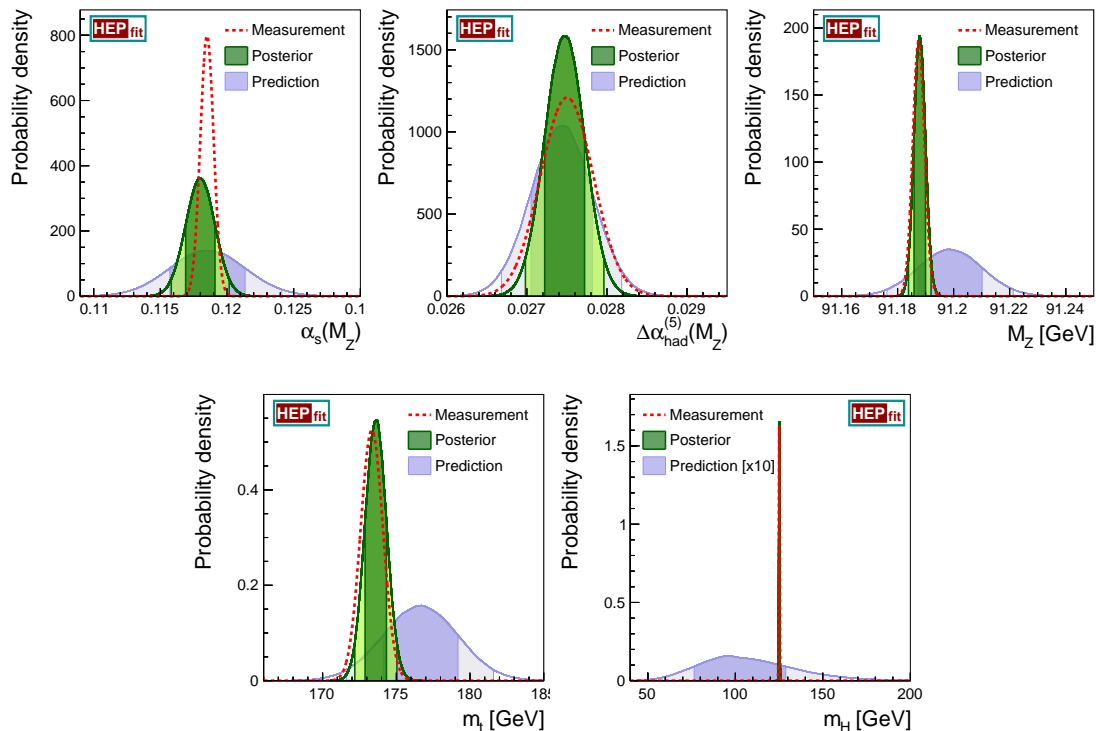


Figure 1. Comparison among the direct measurement, the posterior, and the posterior predictive (or indirect) probability distributions for the input parameters in the SM fit. The latter is obtained from the fit by assuming a flat prior for the parameter under consideration. Dark (light) regions correspond to 68% (95%) probability ranges.

In this case, we remove from the fit one set of correlated observables at a time and compute the prediction for the set of observables together with their correlation matrix. Adding the experimental covariance matrix to the one obtained from the fit, we compute the log likelihood and the corresponding p -value, which we then convert into a global pull for the correlated set of observables assuming Gaussian distributions (nD Pull).

In figure 1, we show a comparison of the direct measurement (*Measurement* in table 1), the posterior probability distribution (*Posterior* in table 1), and the indirect prediction or predictive posterior probability distribution (*Prediction* in table 1) for the five floating input parameters. These plots show at a glance the impact of the precision of each input parameter on the fit, as well as the agreement between the values preferred by the fit and the direct determinations.

Two of the most important observables in the SM fit are the effective mixing angle, $\sin^2 \theta_{\text{eff}}^{\text{lept}}$, and the W mass, M_W . In figure 2 we show the consistency of the predictions for these observables with the direct experimental measurements, their dependence on the top mass, and the impact of other measurements, such as m_H (varied in the range $10 \text{ GeV} < m_H < 1 \text{ TeV}$) and Γ_Z .

Looking at the pulls in table 1, one can notice that there is an overall agreement between EWPO and SM predictions. Only $A_{\text{FB}}^{0,b}$ shows some tension between existing

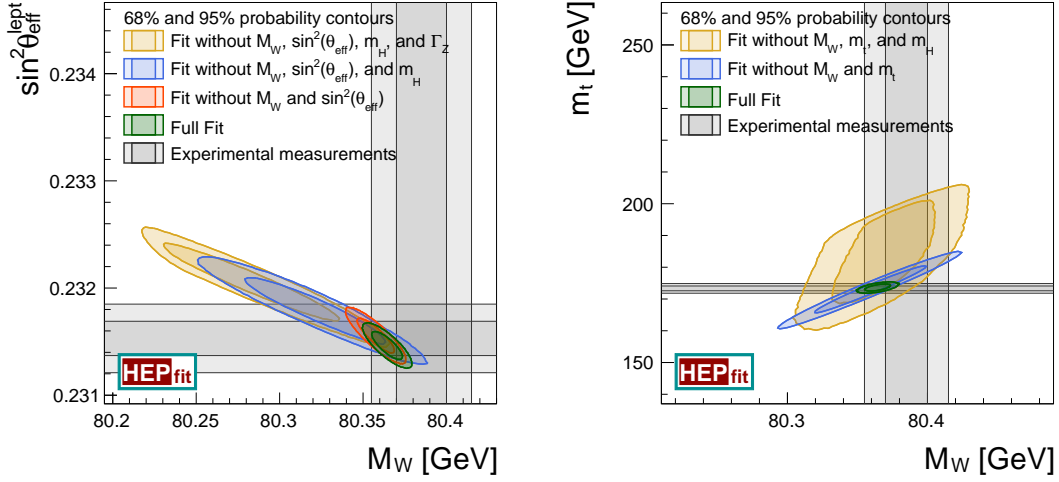


Figure 2. Left: Comparison of the indirect constraints on $\sin^2 \theta_{\text{eff}}^{\text{lept}}$ and M_W with the direct experimental measurements. Dark (light) regions correspond to 68% (95%) probability. Right: The same for m_t and M_W .

	Prediction	α_s	$\Delta\alpha_{\text{had}}^{(5)}$	M_Z	m_t
M_W [GeV]	80.3618 ± 0.0080	± 0.0008	± 0.0060	± 0.0026	± 0.0046
Γ_W [GeV]	2.08849 ± 0.00079	± 0.00048	± 0.00047	± 0.00021	± 0.00036
Γ_Z [GeV]	2.49403 ± 0.00073	± 0.00059	± 0.00031	± 0.00021	± 0.00017
σ_h^0 [nb]	41.4910 ± 0.0062	± 0.0059	± 0.0005	± 0.0020	± 0.0005
$\sin^2 \theta_{\text{eff}}^{\text{lept}}$	0.23148 ± 0.00012	± 0.00000	± 0.00012	± 0.00002	± 0.00002
$P_\tau^{\text{pol}} = \mathcal{A}_\ell$	0.14731 ± 0.00093	± 0.00003	± 0.00091	± 0.00012	± 0.00019
\mathcal{A}_c	0.66802 ± 0.00041	± 0.00001	± 0.00040	± 0.00005	± 0.00008
\mathcal{A}_b	0.934643 ± 0.000076	± 0.000003	± 0.000075	± 0.000010	± 0.000005
$A_{\text{FB}}^{0,\ell}$	0.01627 ± 0.00021	± 0.00001	± 0.00020	± 0.00003	± 0.00004
$A_{\text{FB}}^{0,c}$	0.07381 ± 0.00052	± 0.00002	± 0.00050	± 0.00007	± 0.00010
$A_{\text{FB}}^{0,b}$	0.10326 ± 0.00067	± 0.00002	± 0.00065	± 0.00008	± 0.00013
R_ℓ^0	20.7478 ± 0.0077	± 0.0074	± 0.0020	± 0.0003	± 0.0003
R_c^0	0.172222 ± 0.000026	± 0.000023	± 0.000007	± 0.000001	± 0.000009
R_b^0	0.215800 ± 0.000030	± 0.000013	± 0.000004	± 0.000000	± 0.000026

Table 2. SM predictions computed using the theoretical expressions for the EWPO without the corresponding experimental constraints, and individual uncertainties associated with each input parameter, except for m_H (see text).

measurements and the result of the SM precision fit. Care must be taken when interpreting this as a possible hint of NP, for deviations at this level ($\sim 2\sigma$) are likely to occur when fitting this many observables. Having this in mind, this anomaly will be taken into account in exploring possible parameterizations of NP effects in section 4.

In table 2 we present the full predictions for all EWPO (computed using the theoretical expressions used in the fit without the experimental constraints on the observables) with the breakdown of the parametric uncertainty induced by 1σ variations of the input parameters. We do not include in that table the corresponding column for m_H , since its leading contributions to the EWPO are logarithmic, and hence its error does not induce a significant uncertainty in the predictions. In several cases, the largest contribution to the parametric errors comes from the uncertainty in $\Delta\alpha_{\text{had}}^{(5)}(M_Z)$. This is the dominant source for $\sin^2\theta_{\text{eff}}^{\text{lept}}$ and hence for the different asymmetries. The uncertainties of M_W and the pseudo-observables involving decay widths, on the other hand, receive sizeable contributions from several or all input parameters. In particular, with the new PDG value, $\alpha_s(M_Z)$ becomes the dominant source of uncertainty in all observables involving the hadronic decay width, with the exception of R_b^0 , whose error is controlled by that of m_t .

For the sake of comparison, we repeat the fit using the old PDG determination of $\alpha_s(M_Z)$ and report the results in tables 3 and 4. The effect is particularly visible in all observables involving the hadronic decay width.

	Ref	Measurement	Posterior	Prediction	1D Pull	nD Pull
$\alpha_s(M_Z)$	[9]	0.11850 ± 0.00050	0.11850 ± 0.00049	0.1186 ± 0.0028	0.1	
$\Delta\alpha_{\text{had}}^{(5)}(M_Z)$	[12]	0.02750 ± 0.00033	0.02747 ± 0.00025	0.02743 ± 0.00038	-0.2	
M_Z [GeV]	[13]	91.1875 ± 0.0021	91.1879 ± 0.0021	91.198 ± 0.011	-0.9	
m_t [GeV]	[14]	173.34 ± 0.76	173.61 ± 0.73	176.7 ± 2.5	1.1	
m_H [GeV]	[15]	125.09 ± 0.24	125.09 ± 0.24	102.4 ± 26.4	-0.6	
M_W [GeV]	[16]	80.385 ± 0.015	80.3641 ± 0.0060	80.3601 ± 0.0066	-1.7	
Γ_W [GeV]	[17]	2.085 ± 0.042	2.08893 ± 0.00051	2.08893 ± 0.00051	0.0	
$\sin^2 \theta_{\text{eff}}^{\text{lept}}(Q_{\text{FB}}^{\text{had}})$	[13]	0.2324 ± 0.0012	0.231466 ± 0.000086	0.231437 ± 0.000090	-0.8	
$P_{\tau}^{\text{pol}} = \mathcal{A}_{\ell}$	[13]	0.1465 ± 0.0033	0.14746 ± 0.00068	0.14751 ± 0.00069	0.1	
Γ_Z [GeV]	[13]	2.4952 ± 0.0023	2.49445 ± 0.00040	2.49439 ± 0.00041	0.4	
σ_h^0 [nb]	[13]	41.540 ± 0.037	41.4878 ± 0.0031	41.4880 ± 0.0032	1.3	0.7
R_{ℓ}^0	[13]	20.767 ± 0.025	20.7516 ± 0.0034	20.7513 ± 0.0035	0.6	
$A_{\text{FB}}^{0,\ell}$	[13]	0.0171 ± 0.0010	0.01631 ± 0.00015	0.01627 ± 0.00015	0.9	
\mathcal{A}_{ℓ} (SLD)	[13]	0.1513 ± 0.0021	0.14746 ± 0.00068	0.14762 ± 0.00076	1.7	
\mathcal{A}_c	[13]	0.670 ± 0.027	0.66809 ± 0.00030	0.66816 ± 0.00033	0.03	
\mathcal{A}_b	[13]	0.923 ± 0.020	0.934648 ± 0.000058	0.934661 ± 0.000064	-0.4	
$A_{\text{FB}}^{0,c}$	[13]	0.0707 ± 0.0035	0.07389 ± 0.00037	0.07398 ± 0.00042	-0.9	1.5
$A_{\text{FB}}^{0,b}$	[13]	0.0992 ± 0.0016	0.10337 ± 0.00048	0.10348 ± 0.00054	-2.5	
R_c^0	[13]	0.1721 ± 0.0030	0.172238 ± 0.000013	0.172239 ± 0.000013	-0.1	
R_b^0	[13]	0.21629 ± 0.00066	0.215784 ± 0.000025	0.215783 ± 0.000026	0.8	
$\sin^2 \theta_{\text{eff}}^{ee}$	[18]	0.23248 ± 0.00053			2.1	
$\sin^2 \theta_{\text{eff}}^{\mu\mu}$	[19]	0.2315 ± 0.0010			0.1	
$\sin^2 \theta_{\text{eff}}^{ee}$	[20]	0.23146 ± 0.00047			0.2	
$\sin^2 \theta_{\text{eff}}^{ee,\mu\mu}$	[21]	0.2308 ± 0.0012	0.231466 ± 0.000086	0.231437 ± 0.000090	-0.5	
$\sin^2 \theta_{\text{eff}}^{\mu\mu}$	[22]	0.2287 ± 0.0032			-0.8	
$\sin^2 \theta_{\text{eff}}^{\mu\mu}$	[23]	0.2314 ± 0.0011			-0.3	

Table 3. Same as table 1 using the old PDG determination of $\alpha_s(M_Z)$.

	Prediction	α_s	$\Delta\alpha_{\text{had}}^{(5)}$	M_Z	m_t
M_W [GeV]	80.3615 ± 0.0080	± 0.0003	± 0.0060	± 0.0027	± 0.0046
Γ_W [GeV]	2.08872 ± 0.00066	± 0.00020	± 0.00047	± 0.00021	± 0.00036
Γ_Z [GeV]	2.49433 ± 0.00049	± 0.00025	± 0.00031	± 0.00021	± 0.00017
σ_h^0 [nb]	41.4881 ± 0.0032	± 0.0024	± 0.0005	± 0.0020	± 0.0005
$\sin^2 \theta_{\text{eff}}^{\text{lept}}$	0.23149 ± 0.00012	± 0.00000	± 0.00012	± 0.00002	± 0.00002
$P_\tau^{\text{pol}} = \mathcal{A}_\ell$	0.14730 ± 0.00094	± 0.00001	± 0.00091	± 0.00012	± 0.00019
\mathcal{A}_c	0.66802 ± 0.00041	± 0.00001	± 0.00040	± 0.00005	± 0.00008
\mathcal{A}_b	0.934642 ± 0.000076	± 0.000001	± 0.000075	± 0.000010	± 0.000005
$A_{\text{FB}}^{0,\ell}$	0.01627 ± 0.00021	± 0.00000	± 0.00020	± 0.00003	± 0.00004
$A_{\text{FB}}^{0,c}$	0.07380 ± 0.00052	± 0.00001	± 0.00050	± 0.00007	± 0.00010
$A_{\text{FB}}^{0,b}$	0.10325 ± 0.00067	± 0.00001	± 0.00065	± 0.00008	± 0.00013
R_ℓ^0	20.7515 ± 0.0037	± 0.0031	± 0.0020	± 0.0003	± 0.0003
R_c^0	0.172234 ± 0.000015	± 0.000010	± 0.000007	± 0.000001	± 0.000009
R_b^0	0.215794 ± 0.000027	± 0.000006	± 0.000004	± 0.000000	± 0.000026

Table 4. Same as table 2 using the old PDG determination of $\alpha_s(M_Z)$.

4 Electroweak precision fit beyond the Standard Model

We now generalize the SM fit considering different sets of parameters which account for NP contributions in several extensions of the SM.

4.1 Non-standard oblique corrections

In this section, we use the fit of EWPO to constrain the oblique parameters S , T , U introduced in ref. [31, 32] and the $\varepsilon_{1,2,3,b}$ parameters introduced in refs. [33–35].

The S , T , U parameters account for NP effects in the vacuum-polarization amplitudes of the EW gauge bosons and modify all EWPO considered here. The explicit dependence of the EWPO on S , T , and U can be found in appendix A of ref. [3] where it was also noticed how the EWPO considered here depend only on the following three specific combinations of the S , T , and U parameters (where $s_W = \sin \theta_W$ and $c_W = \cos \theta_W$),

$$\begin{aligned} A &= S - 2c_W^2 T - \frac{(c_W^2 - s_W^2)U}{2s_W^2}, \\ B &= S - 4c_W^2 s_W^2 T, \\ C &= -10(3 - 8s_W^2)S + (63 - 126s_W^2 - 40s_W^4)T. \end{aligned} \tag{4.1}$$

Therefore the extracted values of S , T , and U are correlated. For this reason, we give in tables 5 and 6 the results of the fit together with the correlation matrix. We also remind the reader that A , the only parameter depending on U , describes NP contributions to M_W and Γ_W , the parameter C describes NP contributions to Γ_Z , and NP contributions to all other EWPO are proportional to B . As illustrated in figure 3, S , T , and U are compatible with zero, implying the absence of sizeable oblique corrections beyond those predicted by the SM.

	Result	Correlation Matrix		
S	0.09 ± 0.10	1.00		
T	0.10 ± 0.12	0.86	1.00	
U	0.01 ± 0.09	-0.54	-0.81	1.00

Table 5. Results of the fit for the oblique parameters S , T , and U .

	Result	Correlation Matrix	
S	0.10 ± 0.08	1.00	
T	0.12 ± 0.07	0.86	1.00

Table 6. Results of the fit for the oblique parameters S and T , taking $U = 0$.

Next we consider the $\varepsilon_{1,2,3,b}$ parameters introduced in refs. [33–35]. Unlike the S , T , and U parameters discussed above, the ε_i parameters involve SM contributions associated with the top quark and the Higgs boson, SM flavour non-universal vertex corrections, and further vacuum-polarization corrections [36]. Since the SM is now fully known and there is no need to disentangle top-quark and Higgs-boson contributions anymore, we separate the genuine NP contribution from the SM one by introducing $\delta\varepsilon_i = \varepsilon_i - \varepsilon_{i,\text{SM}}$ for $i = 1, 2, 3, b$, where ε_i are the original parameters and $\varepsilon_{i,\text{SM}}$ contain the SM contribution only. The expressions of the EWPO in terms of $\delta\varepsilon_i$ can be found in ref. [3, 5].

The results of our fit for the $\delta\varepsilon_i$ parameters are summarized in table 7. Some two-dimensional probability distributions are plotted in figure 4. All results are consistent with

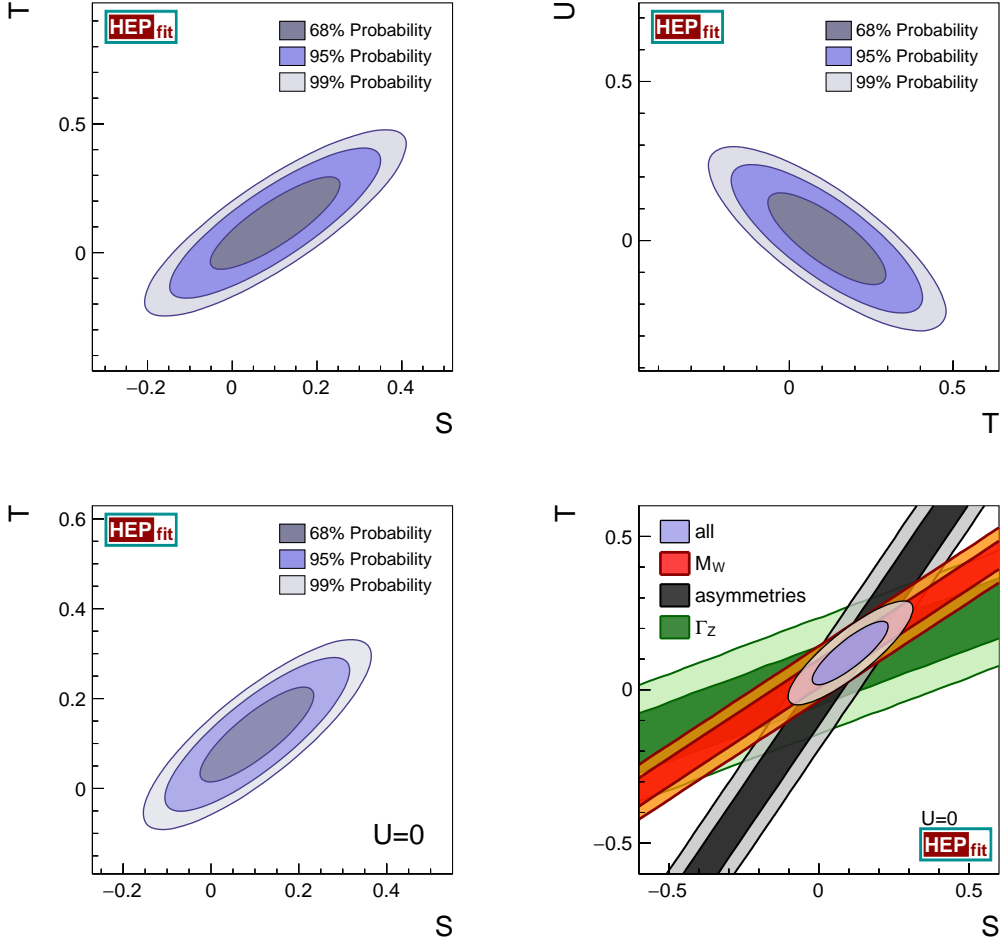


Figure 3. Two-dimensional probability distributions for the oblique parameters S and T (upper-left panel), and T and U (upper-right panel). From darker to lighter the different regions correspond respectively to 68%, 95%, and 99% probability. In the lower panel we show the two-dimensional distributions for S and T fixing $U = 0$, together with the individual constraints from M_W , the asymmetry parameters $\sin^2 \theta_{\text{eff}}^{\text{lept}}$, P_{τ}^{pol} , A_f , and $A_{\text{FB}}^{0,f}$ with $f = \ell, c, b$, and Γ_Z . In this last plot the dark (light) region corresponds to 68% (95%) probability.

the SM. Note that, as mentioned above, the $\delta\varepsilon_i$ parameters include oblique corrections

	Result	Correlation Matrix			
$\delta\varepsilon_1$	0.0007 ± 0.0010	1.00			
$\delta\varepsilon_2$	-0.0002 ± 0.0008	0.82	1.00		
$\delta\varepsilon_3$	0.0007 ± 0.0009	0.87	0.56	1.00	
$\delta\varepsilon_b$	0.0004 ± 0.0013	-0.34	-0.32	-0.24	1.00

Table 7. Results of the fit for the $\delta\varepsilon_i$ parameters ($i = 1, 2, 3, b$).

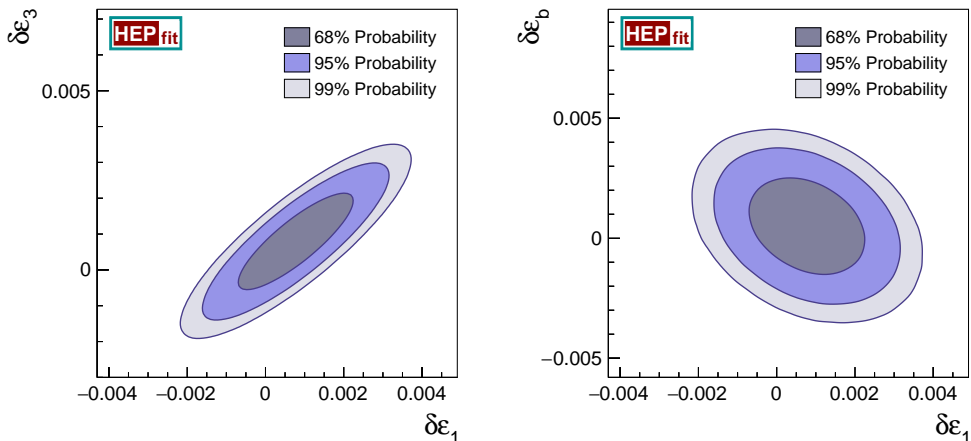


Figure 4. Two-dimensional probability distributions for $\delta\varepsilon_1$ and $\delta\varepsilon_3$ (left), and $\delta\varepsilon_1$ and $\delta\varepsilon_b$ (right) varying all $\delta\varepsilon_i$ parameters. From darker to lighter the different regions correspond to 68%, 95%, and 99% probability.

beyond those connected to the S , T , and U parameters. More precisely,

$$\delta\varepsilon_1 = \alpha T - W + 2X \frac{\sin\theta_W}{\cos\theta_W} - Y \frac{\sin^2\theta_W}{\cos^2\theta_W}, \quad (4.2)$$

$$\delta\varepsilon_2 = -\frac{\alpha}{4\sin^2\theta_W} U - W + 2X \frac{\sin\theta_W}{\cos\theta_W} - V, \quad (4.3)$$

$$\delta\varepsilon_3 = \frac{\alpha}{4\sin^2\theta_W} S - W + \frac{X}{\sin\theta_W \cos\theta_W} - Y, \quad (4.4)$$

where V , W , X , Y are part of the extended set of oblique parameters defined in [36]. With the results in table 7 and the above equations, one can therefore obtain approximate constraints on NP scenarios with vanishing contributions to S , T , and/or U but non-zero values of some of the other parameters (V , W , X , and Y).

4.2 Modified $Zb\bar{b}$ couplings

Motivated by the apparent discrepancy between the SM prediction for $A_{FB}^{0,b}$ and the corresponding experimental result, we also consider here the case where dominant NP contributions appear in the $Zb\bar{b}$ couplings. We parameterize NP contributions to the $Zb\bar{b}$ couplings as follows:

$$g_i^b = g_{i,\text{SM}}^b + \delta g_i^b \quad \text{for } i = L, R \text{ or } V, A, \quad (4.5)$$

and we present results for both V , A , and L , R couplings. Details on the definitions of these couplings can be found in ref. [3]. The EW precision fit finds four solutions for these couplings, but two of them are disfavoured by the off-peak measurement of the forward-backward asymmetry in $e^+e^- \rightarrow b\bar{b}$ [37]. In table 8 and figure 5, we present only the solution closer to the SM. The observed deviations from zero of the parameters δg_i^b reflect the deviation from the SM of the measured value of $A_{FB}^{0,b}$. While the agreement

between the SM and R_b^0 results in a preferred value of δg_L^b consistent with the SM at the 2σ level, a sizeable contribution to δg_R^b is required to explain the $A_{\text{FB}}^{0,b}$, and the resulting 95% probability region in the δg_L^b - δg_R^b plane is only marginally compatible with the SM predictions.

	Result	Correlation Matrix	
δg_R^b	0.016 ± 0.006	1.00	
δg_L^b	0.002 ± 0.001	0.90	1.00
δg_V^b	0.018 ± 0.007	1.00	
δg_A^b	-0.013 ± 0.005	-0.98	1.00

Table 8. Results of the fit for the shifts in the $Zb\bar{b}$ couplings.

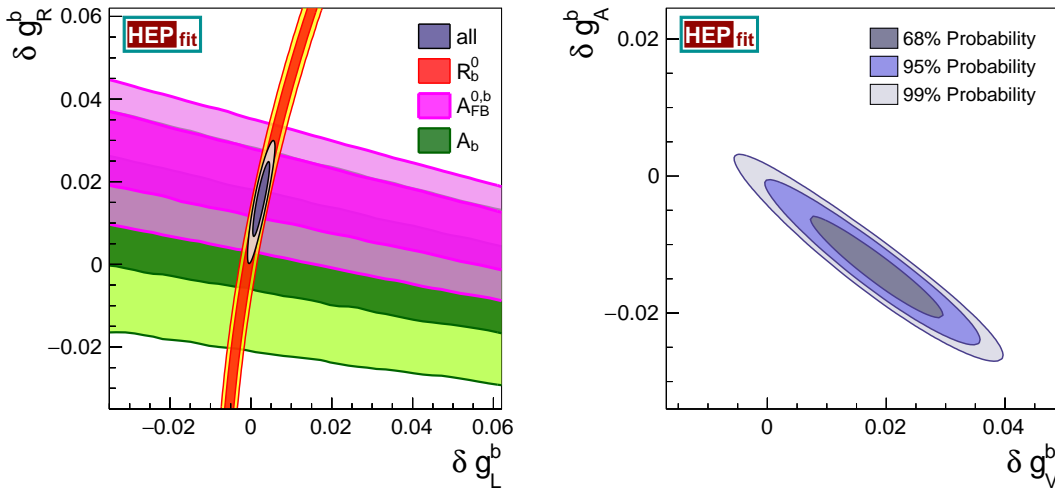


Figure 5. Two-dimensional probability distributions for δg_R^b , δg_L^b (left), and δg_V^b , δg_A^b (right). In the left plot, the dark (light) regions correspond to 68% (95%) probability regions.

4.3 Modified $Zb\bar{b}$ couplings and oblique corrections

In several extensions of the SM, oblique corrections and modifications of the $Zb\bar{b}$ vertex occur simultaneously, possibly affecting only a specific chirality of the vertex (see for example refs. [38, 39]). We therefore consider the following cases: oblique contributions with i) δg_L^b and δg_R^b , ii) δg_L^b only and iii) δg_R^b only. The corresponding results are presented in table 9.

5 Constraints on Higgs-boson couplings

In addition to the standard set of EWPO, we have considered all most recent measurements of Higgs-boson signal strengths, i.e. the ratio between the measured effective cross section and the corresponding SM prediction ($\mu \equiv \sigma/\sigma_{\text{SM}}$), taken from refs. [40, 41] for $H \rightarrow \gamma\gamma$,

	Result	Correlation Matrix			
S	0.04 ± 0.09	1.00			
T	0.08 ± 0.07	0.86	1.00		
δg_L^b	0.003 ± 0.001	-0.24	-0.15	1.00	
δg_R^b	0.017 ± 0.008	-0.29	-0.22	0.91	1.00
$\delta g_R^b = 0$					
S	0.10 ± 0.09	1.00			
T	0.12 ± 0.07	0.85	1.00		
δg_L^b	-0.0001 ± 0.0006	0.07	0.13	1.00	
$\delta g_L^b = 0$					
S	0.08 ± 0.09	1.00			
T	0.10 ± 0.07	0.86	1.00		
δg_R^b	0.004 ± 0.003	-0.19	-0.21	1.00	

Table 9. Results of the combined fit of the oblique parameters S and T , and of the modified $Zb\bar{b}$ couplings, in the case when both δg_R^b and δg_L^b are non zero, and in the case in which either $\delta g_R^b = 0$ or $\delta g_L^b = 0$.

refs. [42, 43] for $H \rightarrow \tau^+\tau^-$, refs. [44–46] for $H \rightarrow ZZ$, refs. [47–49] for $H \rightarrow W^+W^-$, and refs. [50–53] as well as the Tevatron papers [54, 55] for $H \rightarrow b\bar{b}$. The Higgs-boson signal strength μ of a specific Higgs-search analysis can be calculated as

$$\mu = \sum_i w_i r_i \quad \text{with} \quad r_i = \frac{(\sigma \times Br)_i}{(\sigma_{\text{SM}} \times Br_{\text{SM}})_i} \quad \text{and} \quad w_i = \frac{\epsilon_i (\sigma_{\text{SM}} \times Br_{\text{SM}})_i}{\sum_j \epsilon_j (\sigma_{\text{SM}} \times Br_{\text{SM}})_j}, \quad (5.1)$$

where the sum runs over all channels which can contribute to the final state of the specific analysis. The SM Higgs-boson production cross sections (including QCD and, when available, EW corrections) are taken from ref. [56] and the SM Higgs-boson decay rates are taken from ref. [57]. In the presence of NP, the relative experimental efficiencies, ϵ_i , will in general be different from their values in the SM. In particular, the appearance of new tensor structures in the vertices can modify the kinematic distributions of the final-state particles, thereby changing the efficiencies. In this work we only consider rescalings of the SM Higgs couplings and use the SM weight factors throughout. This assumption is justified a posteriori by the overall compatibility of the measurements of Higgs-boson properties with the corresponding SM predictions.

We first consider a minimal scenario consisting of an effective theory with only one Higgs boson below the cutoff scale Λ . We assume that custodial symmetry is approximately realized, and corrections from NP are flavour diagonal and universal. This scenario can be described by a general effective Lagrangian of the form (see e.g. [58–61]):

$$\mathcal{L}_{\text{eff}} = \frac{v^2}{4} \text{tr}(D_\mu \Sigma^\dagger D^\mu \Sigma) \left(1 + 2\kappa_V \frac{H}{v} + \dots \right) - m_i \bar{f}_L^i \left(1 + 2\kappa_f \frac{H}{v} + \dots \right) f_R^i + \dots, \quad (5.2)$$

where v is the vacuum expectation value of the Higgs field, and the longitudinal components of the W and Z bosons, $\chi^a(x)$, are described by the two-by-two matrix $\Sigma(x) =$

$\exp(i\tau^a\chi^a(x)/v)$, with τ^a being the Pauli matrices. The deviations in the Higgs-boson couplings to weak gauge-bosons, HVV ($V = Z, W^\pm$), and to fermions, $Hf\bar{f}$, are parameterized by the scale factors κ_V and κ_f respectively, defined as the ratio between the total Higgs-boson couplings, including NP effects, and the corresponding couplings in the SM (such that $\kappa_V = \kappa_f = 1$ in the SM). We only consider the modification of couplings already existing in the SM and, for loop-induced couplings (Hgg , $H\gamma\gamma$, and $HZ\gamma$), we do not assume NP contributions in loops. For a detailed description of the relations between scale factors and the Higgs-boson signal strengths we refer the reader to ref. [56].

In this context we first perform a fit of the EWPO with the only addition of the scale factor κ_V . The oblique parameters S and T then receive the following contributions [62]:

$$S = \frac{1}{12\pi}(1 - \kappa_V^2) \ln\left(\frac{\Lambda^2}{m_H^2}\right), \quad T = -\frac{3}{16\pi c_W^2}(1 - \kappa_V^2) \ln\left(\frac{\Lambda^2}{m_H^2}\right), \quad (5.3)$$

where $\Lambda = 4\pi v/\sqrt{|1 - \kappa_V^2|}$ is the cutoff scale of the effective Lagrangian. We present the results of the fit for κ_V in table 10 and fig. 6.

The lower bound on κ_V at 95% corresponds to a cutoff scale $\Lambda = 13$ TeV if κ_V is assumed to be smaller than 1, $\Lambda = 8.7$ TeV if κ_V is assumed to be larger than 1, and $\Lambda = 8.8$ TeV marginalizing over the sign of $1 - \kappa_V$. The fit disfavors values of $\kappa_V < 1$ (10% probability), expected for example in composite Higgs models. This problem can be alleviated by adding extra contributions to the oblique parameters [63–66].

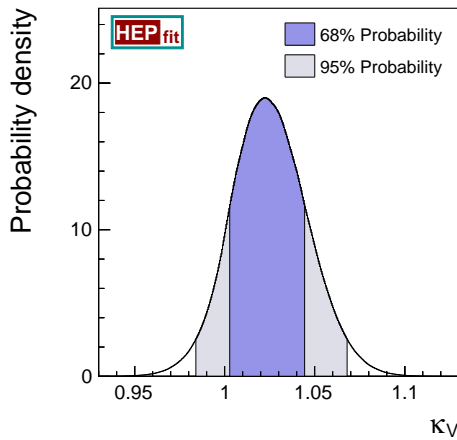


Figure 6. Probability distribution for κ_V derived from precision EW measurements. The dark and light regions correspond respectively to 68% and 95% probabilities.

The two-dimensional probability distributions for κ_V and κ_f obtained from the fit to Higgs-boson signal strengths are summarized in table 11 and shown in figure 7. The

	Result	95% Prob.
κ_V	1.02 ± 0.02	[0.98, 1.07]

Table 10. Results of the fit for the scale factor κ_V at 68% and 95% probabilities.

	Result	95% Prob.	Correlation Matrix	
κ_V	1.01 ± 0.04	[0.93, 1.10]	1.00	
κ_f	1.03 ± 0.10	[0.83, 1.23]	0.31	1.00

Table 11. SM-like solution in the fit of κ_V and κ_f to the Higgs-boson signal strengths.

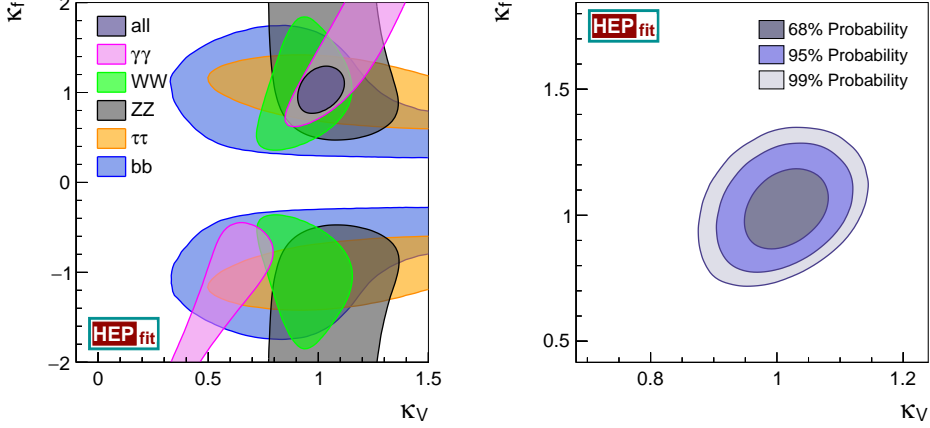


Figure 7. Left: constraints from individual channels at 95% probability. Right: two-dimensional probability distributions for κ_V and κ_f at 68%, 95%, and 99% (darker to lighter), obtained from the fit to the Higgs-boson signal strengths.

	Result	95% Prob.	Correlation Matrix	
κ_V	1.02 ± 0.02	[0.99, 1.06]	1.00	
κ_f	1.03 ± 0.10	[0.85, 1.23]	0.14	1.00

Table 12. Same as table 11 but considering both the Higgs-boson signal strengths and the EWPO.

left panel of of figure 7 shows the 95% probability contours obtained from a fit including only each individual channel (e.g. $H \rightarrow \gamma\gamma$), as well as the result from the global fit. Since both production cross sections and decay rates depend on the modified couplings via products of the form $\kappa_i\kappa_j$, theoretical predictions are symmetric under the simultaneous exchange $\{\kappa_V, \kappa_f\} \leftrightarrow \{-\kappa_V, -\kappa_f\}$. We therefore restrict the parameter space to positive κ_V only. Note also that, when performing the global fit to all channels, the region with negative κ_f is not populated even at 99% probability, so that we only show positive values of κ_f in the right-hand-side plot of figure 7. The effect of performing a combined fit of both Higgs-boson signal strengths and EWPO is summarized in table 12 and illustrated in figure 8 (note that in tables 11 and 12 we only show the results corresponding to the SM-like solution, i.e. $\kappa_{V,f} > 0$). It is interesting to notice that the constraint on κ_V from EWPO is stronger than the one obtained from the Higgs-boson signal strengths alone.

We then lift the assumption of custodial symmetry and rescale the HZZ and HW^+W^- couplings independently, introducing two parameters κ_Z and κ_W , while keeping a unique rescaling factor for all fermionic couplings, κ_f . We obtain the results summarized in table 13 and the corresponding probability distributions shown in figure 9, which are consistent

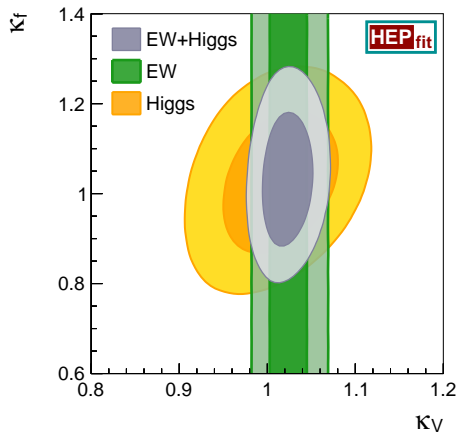


Figure 8. Two-dimensional 68% (dark) and 95% (light) probability contours for κ_V and κ_f (from darker to lighter), obtained from the fit to the Higgs-boson signal strengths and the EWPO.

	Result	95% Prob.	Correlation Matrix		
κ_W	1.00 ± 0.05	[0.89, 1.10]	1.00		
κ_Z	1.07 ± 0.11	[0.85, 1.27]	-0.17	1.00	
κ_f	1.01 ± 0.11	[0.80, 1.22]	0.41	-0.14	1.00

Table 13. SM-like solution in the fit of κ_W , κ_Z , and κ_f to the Higgs-boson signal strengths.

with custodial symmetry. We notice that theoretical predictions are symmetric under the exchanges $\{\kappa_W, \kappa_f\} \leftrightarrow \{-\kappa_W, -\kappa_f\}$ and/or $\kappa_Z \leftrightarrow -\kappa_Z$, where κ_Z can flip the sign independent of κ_W , since the interference between the W and Z contributions to the vector-boson fusion cross section is negligible. Hence we have considered only the parameter space where both κ_W and κ_Z are positive. In this case, we ignore EWPO in the fit, since setting $\kappa_W \neq \kappa_Z$ generates power divergences in the oblique corrections, indicating that the detailed information on the UV theory is necessary for calculating the oblique corrections.

We also consider the case in which we only lift fermion universality and introduce different rescaling factors for charged leptons (κ_ℓ), up-type quarks (κ_u), and down-type quarks (κ_d), while keeping a unique parameter κ_V for both HVV couplings. In this case, from the Higgs-boson signal strengths we obtain the constraints on the scale factors presented in table 14 and in the top plots of figure 10. By adding the EWPO to the fit, the constraints become stronger, as shown in table 15 and in the bottom plots of figure 10. In this case, the Higgs-boson signal strengths are approximately symmetric under the exchanges $\kappa_\ell \leftrightarrow -\kappa_\ell$, $\kappa_d \leftrightarrow -\kappa_d$ and/or $\{\kappa_V, \kappa_u\} \leftrightarrow \{-\kappa_V, -\kappa_u\}$. These approximate symmetries follow from the small effect of the interference between tau and/or bottom-quark loops with top-quark/ W loops in the Higgs-boson decay into two photons, as well as the relatively small interference between bottom- and top-quark loops in gluon-fusion, for $|\kappa_{V,u,d,\ell}| \sim 1$. Moreover, we find that negative values of κ_u are disfavoured in the fit. Hence, in figure 10 we consider only the parameter space where all κ 's are positive. Again,

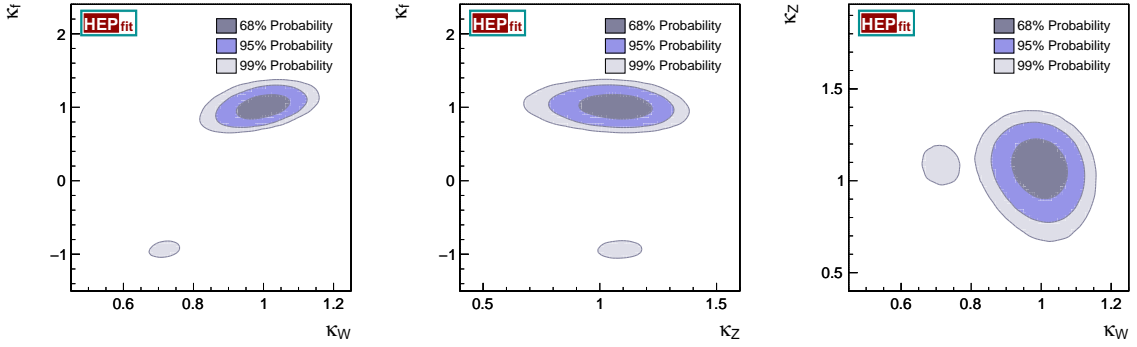


Figure 9. Two-dimensional probability distributions for κ_W and κ_f (left), for κ_Z and κ_f (center), and for κ_W and κ_Z (right) at 68%, 95%, and 99% (darker to lighter), obtained from the fit to the Higgs-boson signal strengths. Note that a small region with $\kappa_f < 0$ is still allowed at 99% probability.

	Result	95% Prob.	Correlation Matrix
κ_V	0.97 ± 0.08	[0.80, 1.13]	1.00
κ_ℓ	1.01 ± 0.14	[0.73, 1.30]	0.54 1.00
κ_u	0.97 ± 0.13	[0.73, 1.25]	0.42 0.41 1.00
κ_d	0.91 ± 0.21	[0.48, 1.35]	0.81 0.61 0.77 1.00

Table 14. SM-like solution in the fit of κ_V , κ_ℓ , κ_u , and κ_d to the Higgs-boson signal strengths.

	Result	95% Prob.	Correlation Matrix
κ_V	1.02 ± 0.02	[0.98, 1.06]	1.00
κ_ℓ	1.07 ± 0.12	[0.82, 1.32]	0.15 1.00
κ_u	1.01 ± 0.12	[0.79, 1.27]	0.10 0.24 1.00
κ_d	1.01 ± 0.13	[0.76, 1.30]	0.31 0.38 0.78 1.00

Table 15. Same as table 14, but considering both the Higgs-boson signal strengths and the EWPO.

the results on table 13 correspond to the SM-like solution, i.e. $\kappa_{V,u,d,\ell} > 0$.

Finally, we consider the case in which both the assumptions of custodial symmetry and fermion universality are lifted, and perform a five-parameter fit of κ_W , κ_Z , κ_ℓ , κ_u , and κ_d reported in table 16. Following the previous discussion, we restrict all the parameters but κ_u (which has an important interference with κ_W in $H \rightarrow \gamma\gamma$) to be positive.

The results presented in this section agree with the recent LHC combination of Higgs couplings in ref. [67], taking into account that the coupling to down quarks in our analysis also includes the Tevatron measurements. See also refs. [68–75] for other recent Higgs couplings analyses.

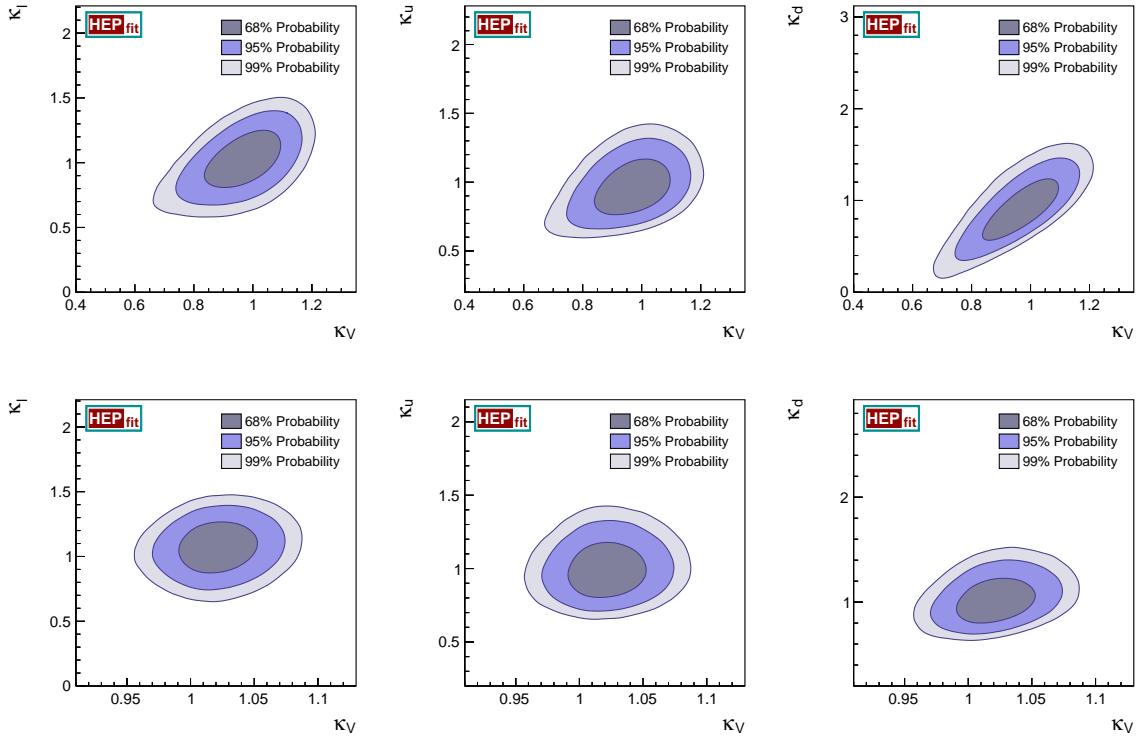


Figure 10. Two-dimensional probability distributions for κ_V and κ_ℓ , for κ_V and κ_u , and for κ_V and κ_d , at 68%, 95%, and 99% (darker to lighter), obtained from the fit to the Higgs-boson signal strengths only (top plots) or the combination of Higgs-boson signal strengths and EWPO (bottom plots).

	Result	95% Prob.	Correlation Matrix
κ_W	0.94 ± 0.10	[0.73, 1.13]	1.00
κ_Z	1.03 ± 0.13	[0.77, 1.28]	0.34 1.00
κ_ℓ	1.02 ± 0.15	[0.73, 1.33]	0.55 0.22 1.00
κ_u	0.95 ± 0.13	$[-0.96, -0.72] \cup [0.68, 1.28]$	0.49 0.04 0.44 1.00
κ_d	0.91 ± 0.22	[0.46, 1.36]	0.81 0.36 0.62 0.78 1.00

Table 16. Results of the simultaneous fit of κ_W , κ_Z , κ_ℓ , κ_u , and κ_d , considering only Higgs-boson signal strengths.

6 Expected sensitivities at future lepton colliders

Future lepton colliders represent an opportunity to reach the ultimate precision both on EWPO and Higgs-boson couplings. In this work, we assess the impact of this improvement in precision by considering the following proposed e^+e^- colliders: the Future Circular Collider (FCCee) project at CERN [76], the International Linear Collider (ILC) in Japan [77, 78], and the Circular Electron Positron Collider (CepC) in China [79]. For completeness in the comparison we also consider the improvements in the measurements of EWPO and Higgs-boson signal strengths expected at the High Luminosity LHC (HL-LHC)

[80–83]. In this section we describe the different physics scenarios we will consider, and estimate the improvements they offer in terms of sensitivity to the different NP models described in sections 4 and 5, comparing the results with those obtained using current data. See refs. [8, 84–86] for earlier analyses of this kind.

Across its years of operation, the FCCee design includes running at the Z pole, and at the WW , HZ , and $t\bar{t}$ production thresholds, with the possibility of a dedicated run at center-of-mass energy $\sqrt{s} \gtrsim 350$ GeV to explore the top-quark couplings. Compared to other options for future e^+e^- colliders, the FCCee also offers the largest integrated luminosity and allows to assess an optimistic best-case scenario. The expected performance of the FCCee machine is documented in refs. [76, 87], and summarized in table 17. The values of integrated luminosity presented there are a useful baseline for our study. Further improvements in performance are under consideration, including an increase in center-of-mass energy. Within the context of our analyses, these improvements would further reduce the statistical uncertainties. On the other hand, since the precision on the observables considered in our study will be mainly dominated by the systematic uncertainties, our conclusions would still hold to a large extent.

FCCee	Z pole	WW threshold	HZ threshold	$t\bar{t}$ threshold	Above $t\bar{t}$ threshold
\sqrt{s} [GeV]	90	160	240	350	> 350
\mathcal{L} [$\text{ab}^{-1}/\text{year}$]	88	15	3.5	1.0	1.0
Years of operation	0.3 / 2.5	1	3	0.5	3
Events	$10^{12}/10^{13}$	10^8	2×10^6	2.1×10^5	7.5×10^4

Table 17. Expected performances of the FCCee machine, taken from Ref. [87]

The ILC project consists of a linear e^+e^- collider optimized for Higgs-boson and top-quark precision measurements, and would initially run at energies $\sqrt{s} = 250, 350, \text{ and } 500$ GeV [77]. The current proposed scenarios would involve approximately 20 years of operation, including a luminosity upgrade. There is also the possibility of extending the energy reach of the machine up to 1 TeV, and we include this in our list of physics scenarios. The energy and luminosity settings of the Higgs-boson runs that we study in this work are given in table 18 [88]. Improved measurements of the properties of the Z lineshape at $\sqrt{s} \approx 91$ GeV, on the other hand, would require a machine upgrade from the Technical Design Report to achieve an optimal luminosity performance [77]. We therefore do not consider this scenario here. As far as EWPO are concerned, we only include the improvements in the Higgs-boson, top-quark, and W masses, where the latter is obtained from the measurements of $e^+e^- \rightarrow W^+W^-$ above threshold with a target overall uncertainty at the level of approximately 3 MeV.

Finally, the CepC project is designed as a Higgs-boson and/or Z factory [79]. Running at $\sqrt{s} \approx 240$ GeV the CepC would produce about 10^6 Higgs-boson particles, allowing measurements of its couplings at the percent level or better. During the $\sqrt{s} \approx 91$ GeV run, on the other hand, up to 10^{11} Z bosons could be produced, improving the sensitivity

ILC	Phase 1			Phase 2 (Luminosity upgrade)		
	\sqrt{s} [GeV]	250	500	1000	250	500
$\int \mathcal{L} dt$ [ab $^{-1}$]	0.25	0.5	1	1.15	1.6	2.5
$\int dt$ (10 7 s)	3	3	3	3	3	3

Table 18. Expected performances of the ILC machine, taken from Ref. [88]

to the Z couplings to the 10^{-4} level. With this statistics, the overall uncertainty for most observables is expected to be dominated by systematic effects. For the run at the Z -pole energy, we will assume a total integrated luminosity larger than 150 fb^{-1} , necessary to achieve the expected precision for all the different EWPO in table 4.1 of ref. [79]. As in the case of the ILC, an improved measurement of the W mass is possible at center-of-mass energies above the W^+W^- production threshold. For the $\sqrt{s} = 250$ GeV run a direct M_W measurement is expected with a similar uncertainty of approximately 3 MeV.

The expected experimental uncertainties on the different EWPO and Higgs-boson signal strengths at the future colliders introduced above are summarized in tables 19 and 20, where we also include projections for the HL-LHC [80–83].

On the theory side, while the theoretical uncertainties associated to unknown higher-order corrections to EWPO in perturbation theory are subdominant compared with current experimental errors, this is no longer the case when we take into account the projected future experimental precision summarized in table 19. The present theoretical uncertainties for the most relevant EWPO are shown in table 21, where we compare them to the corresponding current and future experimental errors. It is clear that we need to improve SM calculations in order for theoretical uncertainties in the predictions of EWPO not to become a limiting factor at future experiments. The future projected theoretical errors in table 21 assume that the complete $\mathcal{O}(\alpha\alpha_s^2)$ corrections, the fermionic $\mathcal{O}(\alpha^2\alpha_s^2)$ and $\mathcal{O}(\alpha^3)$ corrections, and the leading 4-loop corrections entering via the ρ parameter in the different observables will become available [85, 89, 90]. There are other sources of theoretical uncertainties not considered in the previous discussion. First, as explained in section 3, the parametric uncertainties on the theoretical predictions for the different EWPO receive important contributions from the current errors in the experimental measurements of $\Delta\alpha_{\text{had}}^{(5)}(M_Z)$ and $\alpha_s(M_Z)$ (see table 2). Apart from the experimental improvements summarized in table 19, we also assume in all future scenarios that a measurement of $\Delta\alpha_{\text{had}}^{(5)}$ is possible with a precision of $\pm 5 \times 10^{-5}$. Such an improvement is expected to be within the reach of ongoing and future experiments measuring the $e^+e^- \rightarrow \text{hadrons}$ cross section. This requires measuring the ratio R of the hadronic to the muonic e^+e^- cross sections with a relative uncertainty of 1% [91]. Likewise, for the strong coupling constant at the Z pole, we use future lattice QCD projections, which estimate an uncertainty $\delta\alpha_s(M_Z) = \pm 0.0002$ [92]. Another observable which suffers of additional theoretical uncertainties is the top-quark mass. At e^+e^- colliders the top-quark mass can be extracted by reconstructing the $t\bar{t}$ production cross section in a scan around the production thresh-

old. From the shape of the differential cross section one can derive the top-quark mass in different theoretically well-defined schemes, e.g. the potential-subtracted (PS) top-quark mass [93], or the so-called $1S$ top-quark mass [94]. In both schemes the top-quark mass can be extracted with a theoretical uncertainty $\lesssim 50$ MeV [95, 96], to be added to the expected statistical uncertainties shown in table 19. The relation between the PS or $1S$ top-quark mass and the $\overline{\text{MS}}$ top-quark mass has been calculated to 4 loops in perturbative QCD [97], and introduces an additional uncertainty of approximately ~ 20 MeV (~ 10 MeV) in the translation from the PS ($1S$) mass. In our fits we will assume a combined uncertainty in the top-quark mass of 50 MeV for both the ILC and FCCee- $t\bar{t}$ scenarios.

	Current Data	HL-LHC	ILC		FCCee (Run)	CepC
$\alpha_s(M_Z)$	0.1179 \pm 0.0012					
$\Delta\alpha_{\text{had}}^{(5)}(M_Z)$	0.02750 \pm 0.00033					
M_Z [GeV]	91.1875 \pm 0.0021			\pm 0.0001	(FCCee-Z)	\pm 0.0005
m_t [GeV]	173.34 \pm 0.76	\pm 0.6	\pm 0.017	\pm 0.014	(FCCee- $t\bar{t}$)	
m_H [GeV]	125.09 \pm 0.24	\pm 0.05	\pm 0.015	\pm 0.007	(FCCee- HZ)	\pm 0.0059
M_W [GeV]	80.385 \pm 0.015	\pm 0.011	\pm 0.0024	\pm 0.001	(FCCee- WW)	\pm 0.003
Γ_W [GeV]	2.085 \pm 0.042			\pm 0.005	(FCCee- WW)	
Γ_Z [GeV]	2.4952 \pm 0.0023			\pm 0.0001	(FCCee-Z)	\pm 0.0005
σ_h^0 [nb]	41.540 \pm 0.037			\pm 0.025	(FCCee-Z)	\pm 0.037
$\sin^2\theta_{\text{eff}}^{\text{lept}}$	0.2324 \pm 0.0012			\pm 0.0001	(FCCee-Z)	\pm 0.000023
P_τ^{pol}	0.1465 \pm 0.0033			\pm 0.0002	(FCCee-Z)	
A_ℓ	0.1513 \pm 0.0021			\pm 0.000021	(FCCee-Z [pol])	
A_c	0.670 \pm 0.027			\pm 0.01	(FCCee-Z [pol])	
A_b	0.923 \pm 0.020			\pm 0.007	(FCCee-Z [pol])	
$A_{\text{FB}}^{0,\ell}$	0.0171 \pm 0.0010			\pm 0.0001	(FCCee-Z)	\pm 0.0010
$A_{\text{FB}}^{0,c}$	0.0707 \pm 0.0035			\pm 0.0003	(FCCee-Z)	
$A_{\text{FB}}^{0,b}$	0.0992 \pm 0.0016			\pm 0.0001	(FCCee-Z)	\pm 0.00014
R_ℓ^0	20.767 \pm 0.025			\pm 0.001	(FCCee-Z)	\pm 0.007
R_c^0	0.1721 \pm 0.0030			\pm 0.0003	(FCCee-Z)	
R_b^0	0.21629 \pm 0.00066			\pm 0.00006	(FCCee-Z)	\pm 0.00018

Table 19. Expected experimental sensitivities to the different EWPO at future colliders. Apart from the improvements quoted in this table, we also assume that future measurements of $\Delta\alpha_{\text{had}}^{(5)}(M_Z)$ and $\alpha_s(M_Z)$, whose errors dominate in the parametric uncertainties of the theoretical predictions, are possible with an error of approximately $\pm 5 \times 10^{-5}$ and ± 0.0002 , respectively. This assumption is particularly relevant for the FCCee and CepC fits, where the experimental precision for the bulk of electroweak precision measurements will be largely improved.

In what follows we estimate the sensitivity to the different new physics scenarios at the above-mentioned future experiments. To do so, we assume that the future experimental measurements will be fully compatible with the SM predictions. In particular, we use the following reference values of the SM input parameters (see column *Posterior* in table 1),

$$\begin{aligned}
m_H &= 125.09 \text{ GeV}, \quad m_t = 173.61 \text{ GeV}, \quad M_Z = 91.1879 \text{ GeV}, \\
\alpha_s(M_Z) &= 0.1180 \quad \text{and} \quad \Delta\alpha_{\text{had}}^{(5)}(M_Z) = 0.02747,
\end{aligned}
\tag{6.1}$$

	Current	HL-LHC	Phase 1			Phase 2			FCCee	CepC
			ILC			ILC				
			250	500	1000	250	500	1000		
$H \rightarrow b\bar{b}$	$\gtrsim 23\%$	5-36%	1.2%	1.8-28%	0.3-6%	0.56%	0.37-16%	0.3-3.8%	0.2%	0.28%
$H \rightarrow c\bar{c}$			8.3%	6.2-13%	3.1%	3.9%	3.5-7.2%	2%	1.2%	2.2%
$H \rightarrow gg$			7%	4.1-11%	2.3%	3.3%	2.3-6%	1.4%	1.4%	1.6%
$H \rightarrow WW$	$\gtrsim 15\%$	4-11%	6.4%	2.4-9.2%	1.6%	3%	1.3-5.1%	1%	0.9%	1.5%
$H \rightarrow \tau\tau$	$\gtrsim 25\%$	5-15%	4.2%	5.4-9%	3.1%	2%	3-5%	2%	0.7%	1.2%
$H \rightarrow ZZ$	$\gtrsim 24\%$	4-17%	19%	8.2-25%	4.1%	8.8%	4.6-14%	2.6%	3.1%	4.3%
$H \rightarrow \gamma\gamma$	$\gtrsim 20\%$	4-28%	38%	20-38%	7%	16%	13-19%	5.4%	3.0%	9%
$H \rightarrow Z\gamma$		10-27%								
$H \rightarrow \mu\mu$		14-23%			31%			20%	13%	17%

Table 20. Future expected sensitivity to Higgs-boson observables at various future colliders considered in this study.

Observable	Current	Future	Current	ILC	FCC-ee	CepC
	Th. Error	Th. Error	Exp. Error			
M_W [MeV]	4	1	15	3 – 4	1	3
$\sin^2 \theta_{\text{eff}}^{\text{lept}}$ [10^{-5}]	4.5	1.5	16		0.6	2.3
Γ_Z [MeV]	0.5	0.2	2.3		0.1	0.5
R_b^0 [10^{-5}]	15	10	66		6	17

Table 21. Projected theoretical uncertainty for the different EWPO and comparison with the corresponding experimental sensitivity at various future colliders considered in this study.

and take as errors the ones given in Tables 19 and 20. In our analysis we assume that the theoretical calculations necessary to match the experimental precision will be available, and in our fits we use the future projected uncertainties in table 21. To illustrate the impact of theoretical uncertainties, we also consider another scenario where, as in the current EWPO fit, theoretical uncertainties are subdominant and are neglected in the analysis. In this scenario we also assume that the only uncertainty affecting the top-quark mass parameter is the one given in table 19.

With these settings we have performed fits to the main NP scenarios studied in sections 4 and 5, and compared the results with those obtained in a fit assuming the errors of current data.³ The results of the fits to EWPO only are summarized in table 22, while those from the fits to EWPO plus Higgs-boson observables are reported in table 23. In these tables we illustrate the sensitivity to each NP parameter introduced in sections 4 and 5 by showing the $1\text{-}\sigma$ uncertainty on the corresponding parameter from the fit. A comparison of the projected sensitivity on EW parameters and Higgs coupling constants for various future colliders is shown in fig. 11.

From the results in table 22 we observe how the FCCee, with dedicated runs aimed at improving the measurements of the different EWPO, offers the best performance in terms of constraints on NP. We show the results obtained with the Z -pole runs, with and without polarization, and also show the effect of adding the improved measurement of the W mass

³For consistency in the comparison, in this fit we also set the central values to the SM predictions summarized in eq. (6.1).

(WW column) as well as the sensitivity reached after the completion of the whole FCCee program ($t\bar{t}$ column). Several things are apparent from this table. The first one is that, for the NP models considered here, the use of polarized beams at the FCCee would have only a minor impact on the constraining power of the machine. Looking into the results for the different models we observe how, as expected, the major improvement in sensitivity comes from the more precise properties of the Z lineshape. After this first run, one can still achieve notable improvements in the sensitivity to the U parameter ($\delta\varepsilon_2$) from the measurement of M_W (notice that this is essentially the only EWPO that depends on U). Likewise, the sensitivity to κ_V can be reduced by a factor of ~ 2 with the measurement of m_t . This can be understood from eq. (5.3), the lower-right panel of fig. 3, and the positive correlation between M_W and m_t .

In general, the FCCee program would improve current constraints by about an order of magnitude. The CepC also offers good prospects to obtain more stringent NP constraints from EWPO. However, given the information currently available about the machine performance, the CepC bounds would only be a factor of approximately 4-5 better than the bounds derived from current EWPO. Notice also that the current physics program lacks a dedicated run to improve the measurement of the top-quark mass, which plays a significant role in some cases as explained above. In fact, at the ILC, even without a dedicated run at the Z pole, the precise determinations of M_W and m_t are enough to reach the same sensitivity to κ_V as at the CepC.

In table 22 we have also illustrated the effect of the theoretical uncertainties in the results of electroweak fits with the information from future e^+e^- colliders. In this table, the results in the columns with grey background have been computed using the projected theoretical uncertainties, while such uncertainties have been neglected in the columns with white background. As one expects from looking at table 21, the effect of the future theoretical uncertainties on the CepC results are mild, but they are clearly non-negligible compared to the FCCee precision. Indeed, in the case of the FCCee, theoretical uncertainties can reduce the sensitivity to NP in some cases by up to a factor of 2 compared to cases in which the theoretical errors are subdominant.

Finally, in table 23, we show the level of sensitivity to modified Higgs-boson couplings achievable at the various future colliders considered in this study, in the different scenarios explained in section 5. In this case, let us emphasize however that, even before any future lepton collider, the HL-LHC will provide much better determinations of the Higgs-boson properties compared to what has been so far obtained with current data. Using the fermion-universal custodial-symmetric scenario as a reference, i.e. $\kappa_W = \kappa_Z \equiv \kappa_V$ and $\kappa_u = \kappa_d = \kappa_\ell \equiv \kappa_f$, the HL-LHC would be twice as sensitive to deviations from $\kappa_V = 1$, and up to 6-7 times as sensitive to deviations from $\kappa_f = 1$. These results would be further improved at lepton colliders by a factor of 9 (5) for κ_V (κ_f). Focusing on the results obtained at the different lepton colliders we observe how, in general, FCCee and CepC would perform similarly in terms of measuring the Higgs-boson couplings, though the FCCee is somewhat more sensitive to modified couplings to both vector bosons and fermions (in part because of the more precise determination of κ_V via EWPO). At the ILC the results indicate that, assuming custodial symmetry, the initial phase would not be enough to match the FCCee

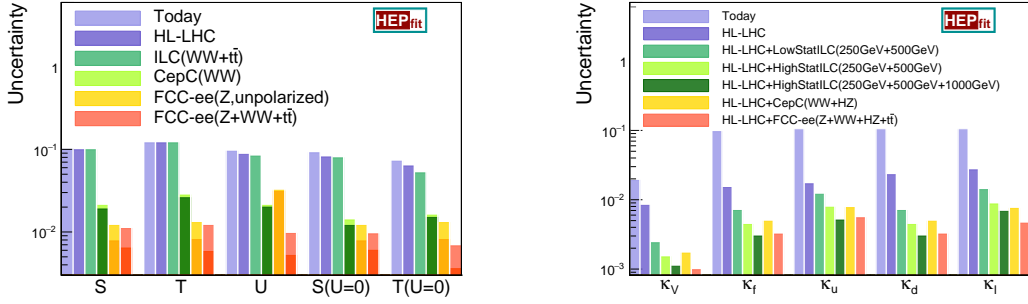


Figure 11. Comparison of expected sensitivities to EW parameters (left) and Higgs couplings (right) from future collider experiments. Different shades of the same colour correspond to results including or neglecting the future theoretical uncertainties.

or CepC precision. Matching the CepC would be possible after a luminosity upgrade even in the absence of a dedicated run at $\sqrt{s} = 1$ TeV. Including such a run in the physics program would make the ILC the best overall machine for the determination of the Higgs-boson properties (one exception would be the couplings to leptons, where the FCCee still offers the more precise measurement). In particular, while the FCCee and the CepC Higgs-boson runs will only explore center-of-mass energies $\sqrt{s} \approx 240$ GeV, where Higgs-boson production occurs mostly via ZH associated production, running at the ILC with $\sqrt{s} = 500$ GeV or $\sqrt{s} = 1000$ GeV gives also access to W -boson fusion production, as well as $t\bar{t}H$ associated production. This results in a determination of κ_W approximately 10 times more precise than at the FCCee/CepC.

	Current		HL-LHC		ILC		FCCee			CepC				
							Z (no pol)	Z (pol)	WW	$t\bar{t}$				
ΔS [$\times 10^{-3}$]	100	99	99	99	99	99	12	11	11	6.4	11	6.3	21	19
ΔT [$\times 10^{-3}$]	120	120	120	120	120	120	13	13	13	7.9	12	5.8	28	26
ΔU [$\times 10^{-3}$]	95	87	83	82	82	82	32	31	31	9.8	5.4	9.6	21	20
ΔS [$\times 10^{-3}$]	91	81	79	79	79	79	12	11	11	6.4	9.5	6.1	14	12
ΔT [$\times 10^{-3}$]	72	63	52	52	52	52	13	13	10	7.4	6.8	3.6	16	15
$(U=0)$														
$\Delta \varepsilon_1^{\text{NP}}$ [$\times 10^{-5}$]	96	96	96	95	95	95	11	11	11	7.2	11	7.2	9.5	23
$\Delta \varepsilon_2^{\text{NP}}$ [$\times 10^{-5}$]	86	81	77	76	76	76	29	28	28	8.6	8.6	4.8	21	19
$\Delta \varepsilon_3^{\text{NP}}$ [$\times 10^{-5}$]	91	87	88	87	87	87	9.9	9.3	9.2	5.5	9.2	5.5	20	18
$\Delta \varepsilon_b^{\text{NP}}$ [$\times 10^{-5}$]	130	130	130	130	130	130	15	15	15	12	15	12	14	37
$\Delta \delta g_L^b$ [$\times 10^{-4}$]	14	14	14	14	14	14	1.5	1.2	1.1	1.2	1.1	1.1	1.2	2.2
$\Delta \delta g_R^b$ [$\times 10^{-4}$]	72	70	70	70	70	70	7.1	5.3	5.3	5.3	5.3	5.3	8.9	8.6
$\Delta \kappa_V$ [$\times 10^{-3}$]	22	14	4.5	4.4	4.4	4.4	4.6	4.4	3.7	4.1	3.7	1.8	5	4.7

Table 22. Comparison of the current and expected sensitivities, Δ , to the different NP scenarios at the future colliders considered in this study. In this table, the future projections for the sensitivity to κ_V has been computed considering only the improvements in EWPO. (See table 23 for the projections using EWPO and Higgs-boson observables.) For the case of future lepton colliders we quote results that also include the expected future theoretical errors given in table 21 (dark background), as well as results in which the theoretical errors have been neglected (white background).

	Current	HL-LHC	ILC ²⁵⁰ ₅₀₀		ILC ²⁵⁰ ₅₀₀		ILC ²⁵⁰ ₅₀₀ ²⁵⁰ ₁₀₀₀		CepC
			Low stats	High stats	High stats	High stats			
$\Delta\kappa_V [\times 10^{-4}]$	190	83	24	15	11	9.8 (8.7)	17		
$\Delta\kappa_f [\times 10^{-4}]$	960	150	70	44	30	32	49		
$\Delta\kappa_W [\times 10^{-4}]$	510	120	33	19	12	91	100		
$\Delta\kappa_Z [\times 10^{-4}]$	1100	150	46	25	23	12	18		
$\Delta\kappa_f [\times 10^{-4}]$	1100	160	71	45	30	90	100		
$\Delta\kappa_V [\times 10^{-4}]$	210	120	25 (24)	16	12	10 (9)	17		
$\Delta\kappa_u [\times 10^{-4}]$	1200	170	120	78	51	55	77		
$\Delta\kappa_d [\times 10^{-4}]$	1400	230	70	44	30	32	49		
$\Delta\kappa_\ell [\times 10^{-4}]$	1300	270	140	87	68	46	75		

Table 23. Comparison of the current and expected sensitivities, Δ , to modified Higgs-boson couplings at the future colliders considered in this study. Results have been obtained using the improvements in both the Higgs-boson signal strengths and the EWPO (for κ_V). The latter are only included in the scenarios with $\kappa_W = \kappa_Z = \kappa_V$. The EWPO used in this table have been computed including the projected future theoretical uncertainties in the precision observables. Neglecting these only seems to have a noticeable effect on the FCCee results, as this is the only case where the EWPO determination of κ_V is precise enough to have an impact in the combination with Higgs-boson data. In this case only we quote in parenthesis the results obtained assuming subdominant theoretical uncertainties in the EWPO. The projections for the sensitivities to Higgs-boson observables at future lepton colliders (ILC, FCCee and CepC) also include the information from the expected improvement in the Higgs-boson signal strengths at the HL-LHC.

7 Conclusions

With the discovery of a SM-like Higgs boson during Run I of the LHC, the possibility of using EW and Higgs-boson precision measurements as a portal to NP has become a reality. Through the steady improvement of both theoretical and experimental accuracies, electroweak and Higgs-boson precision physics could lead us a long way towards determining the UV completion of the SM and the more fundamental origin of the spontaneously-broken realization of the electroweak symmetry.

Indirect searches for NP are indeed as important as ever in the physics program of Run II of the LHC: they will probe physics at inaccessible high scales and provide clues on the nature of new particles. In this context, it is very valuable, if not essential, to provide a complete and consistent framework in which all available experimental data, from precision measurements of electroweak observables and Higgs-boson couplings to flavour-physics results, can be analyzed to constrain the theory in a statistically significant way.

The study presented in this paper illustrates how this can be achieved in the context of the `HEPfit` package, and provides results for a global fit of EWPO and Higgs-boson signal-strength measurements obtained from LHC Run I data collected at 7 and 8 TeV.

At the moment, the constraints derived for Higgs-boson couplings to SM gauge bosons and fermions are overall compatible with SM predictions within the current accuracy. From the results of section 5 we see that the combined study of EWPO and Higgs-boson observables can provide more stringent constraints on Higgs-boson couplings. We can foresee that the higher statistics expected in Run II of the LHC will offer the possibility to isolate potential NP effects from global fits of SM precision observables. This will become even more crucial at the HL-LHC and at a future generation of e^+e^- colliders (FCCee, ILC, CepC) where very high experimental precision for EWPO and Higgs-boson couplings will be achievable. We have dedicated a section of this paper to a study of the sensitivity of different future experimental facilities to NP effects, and have determined at what point more accurate theoretical predictions will be needed.

Finally, we notice that deviations from the SM predictions of EWPO and Higgs-boson couplings constitute indirect evidence of new physics that still need to be interpreted in terms of specific physical degrees of freedom. A more refined theoretical approach, which entails a generalization of the SM Lagrangian to systematically include all effective interactions generated by the presence of NP at the UV scale, will then be necessary in order to explore the nature of such deviations. In a following paper [7] we will explore the possibility of using an effective field theory approach to build a model-independent study of NP effects in Higgs-boson couplings and use the `HEPfit` framework to combine it with a fit of all available electroweak precision data.

Acknowledgments

M. C. is associated to the Dipartimento di Matematica e Fisica, Università di Roma Tre, and E. F. and L. S. are associated to the Dipartimento di Fisica, Università di Roma “La Sapienza”. The research leading to these results has received funding from the European

Research Council under the European Union’s Seventh Framework Programme (FP/2007-2013) / grants n. 267985 and n. 279972. The work of L. R. is supported in part by the U.S. Department of Energy under grant DE-SC0010102, and by the National Science Foundation under Grant No. NSF PHY11-25915. L. R. would like to thank the Kavli Institute for Theoretical Physics (UCSB) for hospitality while this work was being completed.

References

- [1] HEPfit Collaboration, *HEPfit: a Code for the Combination of Indirect and Direct Constraints on High Energy Physics Models*, in preparation.
- [2] HEPfit Collaboration, <http://hepfit.roma1.infn.it>.
- [3] M. Ciuchini, E. Franco, S. Mishima, and L. Silvestrini, *Electroweak Precision Observables, New Physics and the Nature of a 126 GeV Higgs Boson*, *JHEP* **08** (2013) 106, [[arXiv:1306.4644](https://arxiv.org/abs/1306.4644)].
- [4] J. de Blas, M. Ciuchini, E. Franco, D. Ghosh, S. Mishima, M. Pierini, L. Reina, and L. Silvestrini, *Global Bayesian Analysis of the Higgs-boson Couplings*, in *International Conference on High Energy Physics 2014 (ICHEP 2014) Valencia, Spain, July 2-9, 2014*. [[arXiv:1410.4204](https://arxiv.org/abs/1410.4204)].
- [5] M. Ciuchini, E. Franco, S. Mishima, M. Pierini, L. Reina, and L. Silvestrini, *Update of the electroweak precision fit, interplay with Higgs-boson signal strengths and model-independent constraints on new physics*, in *International Conference on High Energy Physics 2014 (ICHEP 2014) Valencia, Spain, July 2-9, 2014*. [[arXiv:1410.6940](https://arxiv.org/abs/1410.6940)].
- [6] J. de Blas, M. Ciuchini, E. Franco, D. Ghosh, S. Mishima, M. Pierini, L. Reina, and L. Silvestrini, *Updates on fits to electroweak parameters*, in *27th International Symposium on Lepton Photon Interactions at High Energy (LP15), Ljubljana, Slovenia, August 17-22, 2015*. To appear in the Proceedings.
- [7] J. de Blas, M. Ciuchini, E. Franco, D. Ghosh, S. Mishima, M. Pierini, L. Reina, and L. Silvestrini. in preparation.
- [8] **Gfitter Group** Collaboration, M. Baak, J. Cúth, J. Haller, A. Hoecker, R. Kogler, K. Mönig, M. Schott, and J. Stelzer, *The global electroweak fit at NNLO and prospects for the LHC and ILC*, *Eur. Phys. J.* **C74** (2014) 3046, [[arXiv:1407.3792](https://arxiv.org/abs/1407.3792)].
- [9] **Particle Data Group** Collaboration, K. A. Olive et al., *Review of Particle Physics*, *Chin. Phys.* **C38** (2014) 090001 and 2015 update.
- [10] A. Caldwell, D. Kollar, and K. Kroninger, *BAT: The Bayesian Analysis Toolkit*, *Comput. Phys. Commun.* **180** (2009) 2197–2209, [[arXiv:0808.2552](https://arxiv.org/abs/0808.2552)].
- [11] A. Akhundov, A. Arbuzov, S. Riemann, and T. Riemann, *The ZFITTER project*, *Phys. Part. Nucl.* **45** (2014), no. 3 529–549, [[arXiv:1302.1395](https://arxiv.org/abs/1302.1395)].
- [12] H. Burkhardt and B. Pietrzyk, *Recent BES measurements and the hadronic contribution to the QED vacuum polarization*, *Phys. Rev.* **D84** (2011) 037502, [[arXiv:1106.2991](https://arxiv.org/abs/1106.2991)].
- [13] **SLD Electroweak Group, DELPHI, ALEPH, SLD, SLD Heavy Flavour Group, OPAL, LEP Electroweak Working Group, L3** Collaboration, S. Schael et al., *Precision electroweak measurements on the Z resonance*, *Phys. Rept.* **427** (2006) 257–454, [[hep-ex/0509008](https://arxiv.org/abs/hep-ex/0509008)].

- [14] **ATLAS, CDF, CMS, D0** Collaboration, *First combination of Tevatron and LHC measurements of the top-quark mass*, [arXiv:1403.4427](#).
- [15] **ATLAS, CMS** Collaboration, G. Aad et al., *Combined Measurement of the Higgs Boson Mass in pp Collisions at $\sqrt{s} = 7$ and 8 TeV with the ATLAS and CMS Experiments*, *Phys. Rev. Lett.* **114** (2015) 191803, [[arXiv:1503.07589](#)].
- [16] **CDF, D0** Collaboration, T. E. W. Group, *2012 Update of the Combination of CDF and D0 Results for the Mass of the W Boson*, [arXiv:1204.0042](#).
- [17] **Tevatron Electroweak Working Group, CDF, DELPHI, SLD Electroweak and Heavy Flavour Groups, ALEPH, LEP Electroweak Working Group, SLD, OPAL, D0, L3** Collaboration, L. E. W. Group, *Precision Electroweak Measurements and Constraints on the Standard Model*, [arXiv:1012.2367](#).
- [18] **CDF** Collaboration, T. A. Aaltonen et al., *Measurement of $\sin^2 \theta_{\text{eff}}^{\text{lept}}$ using e^+e^- pairs from γ^*/Z bosons produced in $p\bar{p}$ collisions at a center-of-momentum energy of 1.96 TeV*, [arXiv:1605.02719](#).
- [19] **CDF** Collaboration, T. A. Aaltonen et al., *Indirect measurement of $\sin^2 \theta_W$ (or M_W) using $\mu^+\mu^-$ pairs from γ^*/Z bosons produced in $p\bar{p}$ collisions at a center-of-momentum energy of 1.96 TeV*, *Phys. Rev.* **D89** (2014), no. 7 072005, [[arXiv:1402.2239](#)].
- [20] **D0** Collaboration, V. M. Abazov et al., *Measurement of the effective weak mixing angle in $p\bar{p} \rightarrow Z/\gamma^* \rightarrow e^+e^-$ events*, *Phys. Rev. Lett.* **115** (2015), no. 4 041801, [[arXiv:1408.5016](#)].
- [21] **ATLAS** Collaboration, G. Aad et al., *Measurement of the forward-backward asymmetry of electron and muon pair-production in pp collisions at $\sqrt{s} = 7$ TeV with the ATLAS detector*, *JHEP* **09** (2015) 049, [[arXiv:1503.03709](#)].
- [22] **CMS** Collaboration, S. Chatrchyan et al., *Measurement of the weak mixing angle with the Drell-Yan process in proton-proton collisions at the LHC*, *Phys. Rev.* **D84** (2011) 112002, [[arXiv:1110.2682](#)].
- [23] **LHCb** Collaboration, R. Aaij et al., *Measurement of the forward-backward asymmetry in $Z/\gamma^* \rightarrow \mu^+\mu^-$ decays and determination of the effective weak mixing angle*, *JHEP* **11** (2015) 190, [[arXiv:1509.07645](#)].
- [24] A. Freitas, *Higher-order electroweak corrections to the partial widths and branching ratios of the Z boson*, *JHEP* **04** (2014) 070, [[arXiv:1401.2447](#)].
- [25] Y. Schroder and M. Steinhauser, *Four-loop singlet contribution to the rho parameter*, *Phys. Lett.* **B622** (2005) 124–130, [[hep-ph/0504055](#)].
- [26] K. G. Chetyrkin, M. Faisst, J. H. Kuhn, P. Maierhofer, and C. Sturm, *Four-Loop QCD Corrections to the Rho Parameter*, *Phys. Rev. Lett.* **97** (2006) 102003, [[hep-ph/0605201](#)].
- [27] R. Boughezal and M. Czakon, *Single scale tadpoles and $O(G_F m_t^2 \alpha_s^3)$ corrections to the ρ parameter*, *Nucl. Phys.* **B755** (2006) 221–238, [[hep-ph/0606232](#)].
- [28] M. Awramik, M. Czakon, A. Freitas, and G. Weiglein, *Precise prediction for the W boson mass in the standard model*, *Phys. Rev.* **D69** (2004) 053006, [[hep-ph/0311148](#)].
- [29] **CMS** Collaboration, S. Chatrchyan et al., *Determination of the top-quark pole mass and strong coupling constant from the t t -bar production cross section in pp collisions at $\sqrt{s} = 7$ TeV*, *Phys. Lett.* **B728** (2014) 496–517, [[arXiv:1307.1907](#)]. [Erratum: *Phys. Lett.* **B738**, 526(2014)].

- [30] S. Aoki et al., *Review of lattice results concerning low-energy particle physics*, [arXiv:1607.00299](#).
- [31] M. E. Peskin and T. Takeuchi, *A New constraint on a strongly interacting Higgs sector*, *Phys. Rev. Lett.* **65** (1990) 964–967.
- [32] M. E. Peskin and T. Takeuchi, *Estimation of oblique electroweak corrections*, *Phys. Rev.* **D46** (1992) 381–409.
- [33] G. Altarelli and R. Barbieri, *Vacuum polarization effects of new physics on electroweak processes*, *Phys. Lett.* **B253** (1991) 161–167.
- [34] G. Altarelli, R. Barbieri, and S. Jadach, *Toward a model independent analysis of electroweak data*, *Nucl. Phys.* **B369** (1992) 3–32. [Erratum: *Nucl. Phys.*B376,444(1992)].
- [35] G. Altarelli, R. Barbieri, and F. Caravaglios, *Nonstandard analysis of electroweak precision data*, *Nucl. Phys.* **B405** (1993) 3–23.
- [36] R. Barbieri, A. Pomarol, R. Rattazzi, and A. Strumia, *Electroweak symmetry breaking after LEP-1 and LEP-2*, *Nucl. Phys.* **B703** (2004) 127–146, [[hep-ph/0405040](#)].
- [37] D. Choudhury, T. M. P. Tait, and C. E. M. Wagner, *Beautiful mirrors and precision electroweak data*, *Phys. Rev.* **D65** (2002) 053002, [[hep-ph/0109097](#)].
- [38] C. Grojean, O. Matsedonskyi, and G. Panico, *Light top partners and precision physics*, *JHEP* **10** (2013) 160, [[arXiv:1306.4655](#)].
- [39] D. Ghosh, M. Salvarezza, and F. Senia, *Extending the Analysis of Electroweak Precision Constraints in Composite Higgs Models*, [arXiv:1511.08235](#).
- [40] **ATLAS** Collaboration, G. Aad et al., *Measurement of Higgs boson production in the diphoton decay channel in pp collisions at center-of-mass energies of 7 and 8 TeV with the ATLAS detector*, *Phys. Rev.* **D90** (2014), no. 11 112015, [[arXiv:1408.7084](#)].
- [41] **CMS** Collaboration, V. Khachatryan et al., *Observation of the diphoton decay of the Higgs boson and measurement of its properties*, *Eur. Phys. J.* **C74** (2014), no. 10 3076, [[arXiv:1407.0558](#)].
- [42] **ATLAS** Collaboration, G. Aad et al., *Evidence for the Higgs-boson Yukawa coupling to tau leptons with the ATLAS detector*, *JHEP* **04** (2015) 117, [[arXiv:1501.04943](#)].
- [43] **CMS** Collaboration, S. Chatrchyan et al., *Evidence for the 125 GeV Higgs boson decaying to a pair of τ leptons*, *JHEP* **05** (2014) 104, [[arXiv:1401.5041](#)].
- [44] **ATLAS** Collaboration, G. Aad et al., *Measurements of Higgs boson production and couplings in the four-lepton channel in pp collisions at center-of-mass energies of 7 and 8 TeV with the ATLAS detector*, *Phys. Rev.* **D91** (2015), no. 1 012006, [[arXiv:1408.5191](#)].
- [45] **CMS** Collaboration, S. Chatrchyan et al., *Measurement of the properties of a Higgs boson in the four-lepton final state*, *Phys. Rev.* **D89** (2014), no. 9 092007, [[arXiv:1312.5353](#)].
- [46] **CMS** Collaboration, V. Khachatryan et al., *Precise determination of the mass of the Higgs boson and tests of compatibility of its couplings with the standard model predictions using proton collisions at 7 and 8 TeV*, *Eur. Phys. J.* **C75** (2015), no. 5 212, [[arXiv:1412.8662](#)].
- [47] **ATLAS** Collaboration, G. Aad et al., *Observation and measurement of Higgs boson decays to WW^* with the ATLAS detector*, *Phys. Rev.* **D92** (2015), no. 1 012006, [[arXiv:1412.2641](#)].

- [48] **ATLAS** Collaboration, G. Aad et al., *Study of $(W/Z)H$ production and Higgs boson couplings using $H \rightarrow WW^*$ decays with the ATLAS detector*, *JHEP* **08** (2015) 137, [[arXiv:1506.06641](#)].
- [49] **CMS** Collaboration, S. Chatrchyan et al., *Measurement of Higgs boson production and properties in the WW decay channel with leptonic final states*, *JHEP* **01** (2014) 096, [[arXiv:1312.1129](#)].
- [50] **ATLAS** Collaboration, G. Aad et al., *Search for the $b\bar{b}$ decay of the Standard Model Higgs boson in associated $(W/Z)H$ production with the ATLAS detector*, *JHEP* **01** (2015) 069, [[arXiv:1409.6212](#)].
- [51] **ATLAS** Collaboration, G. Aad et al., *Search for the Standard Model Higgs boson produced in association with top quarks and decaying into $b\bar{b}$ in pp collisions at $\sqrt{s} = 8$ TeV with the ATLAS detector*, *Eur. Phys. J.* **C75** (2015), no. 7 349, [[arXiv:1503.05066](#)].
- [52] **CMS** Collaboration, S. Chatrchyan et al., *Search for the standard model Higgs boson produced in association with a W or a Z boson and decaying to bottom quarks*, *Phys. Rev.* **D89** (2014), no. 1 012003, [[arXiv:1310.3687](#)].
- [53] **CMS** Collaboration, V. Khachatryan et al., *Search for the associated production of the Higgs boson with a top-quark pair*, *JHEP* **09** (2014) 087, [[arXiv:1408.1682](#)]. [Erratum: *JHEP*10,106(2014)].
- [54] **CDF** Collaboration, T. Aaltonen et al., *Combination fo Searches for the Higgs Boson Using the Full CDF Data Set*, *Phys. Rev.* **D88** (2013), no. 5 052013, [[arXiv:1301.6668](#)].
- [55] **D0** Collaboration, V. M. Abazov et al., *Combined search for the Higgs boson with the D0 experiment*, *Phys. Rev.* **D88** (2013), no. 5 052011, [[arXiv:1303.0823](#)].
- [56] **LHC Higgs Cross Section Working Group** Collaboration, J. R. Andersen et al., *Handbook of LHC Higgs Cross Sections: 3. Higgs Properties*, [arXiv:1307.1347](#).
- [57] R. Contino, M. Ghezzi, C. Grojean, M. Mühlleitner, and M. Spira, *eHDECAY: an Implementation of the Higgs Effective Lagrangian into HDECAY*, *Comput. Phys. Commun.* **185** (2014) 3412–3423, [[arXiv:1403.3381](#)].
- [58] G. F. Giudice, C. Grojean, A. Pomarol, and R. Rattazzi, *The Strongly-Interacting Light Higgs*, *JHEP* **06** (2007) 045, [[hep-ph/0703164](#)].
- [59] R. Contino, C. Grojean, M. Moretti, F. Piccinini, and R. Rattazzi, *Strong Double Higgs Production at the LHC*, *JHEP* **05** (2010) 089, [[arXiv:1002.1011](#)].
- [60] A. Azatov, R. Contino, and J. Galloway, *Model-Independent Bounds on a Light Higgs*, *JHEP* **04** (2012) 127, [[arXiv:1202.3415](#)]. [Erratum: *JHEP*04,140(2013)].
- [61] R. Contino, M. Ghezzi, C. Grojean, M. Mühlleitner, and M. Spira, *Effective Lagrangian for a light Higgs-like scalar*, *JHEP* **07** (2013) 035, [[arXiv:1303.3876](#)].
- [62] R. Barbieri, B. Bellazzini, V. S. Rychkov, and A. Varagnolo, *The Higgs boson from an extended symmetry*, *Phys. Rev.* **D76** (2007) 115008, [[arXiv:0706.0432](#)].
- [63] C. Grojean, W. Skiba, and J. Terning, *Disguising the oblique parameters*, *Phys. Rev.* **D73** (2006) 075008, [[hep-ph/0602154](#)].
- [64] A. Azatov, R. Contino, A. Di Iura, and J. Galloway, *New Prospects for Higgs Compositeness in $h \rightarrow Z\gamma$* , *Phys. Rev.* **D88** (2013), no. 7 075019, [[arXiv:1308.2676](#)].

- [65] A. Pich, I. Rosell, and J. J. Sanz-Cillero, *Viability of strongly-coupled scenarios with a light Higgs-like boson*, *Phys. Rev. Lett.* **110** (2013) 181801, [[arXiv:1212.6769](#)].
- [66] A. Pich, I. Rosell, and J. J. Sanz-Cillero, *Oblique S and T Constraints on Electroweak Strongly-Coupled Models with a Light Higgs*, *JHEP* **01** (2014) 157, [[arXiv:1310.3121](#)].
- [67] **ATLAS, CMS Collaboration**, G. Aad et al., *Measurements of the Higgs boson production and decay rates and constraints on its couplings from a combined ATLAS and CMS analysis of the LHC pp collision data at $\sqrt{s} = 7$ and 8 TeV*, [arXiv:1606.02266](#).
- [68] A. Falkowski, F. Riva, and A. Urbano, *Higgs at last*, *JHEP* **11** (2013) 111, [[arXiv:1303.1812](#)].
- [69] J. Ellis and T. You, *Updated Global Analysis of Higgs Couplings*, *JHEP* **06** (2013) 103, [[arXiv:1303.3879](#)].
- [70] A. Djouadi and G. Moreau, *The couplings of the Higgs boson and its CP properties from fits of the signal strengths and their ratios at the 7+8 TeV LHC*, *Eur. Phys. J.* **C73** (2013), no. 9 2512, [[arXiv:1303.6591](#)].
- [71] G. Belanger, B. Dumont, U. Ellwanger, J. F. Gunion, and S. Kraml, *Global fit to Higgs signal strengths and couplings and implications for extended Higgs sectors*, *Phys. Rev.* **D88** (2013) 075008, [[arXiv:1306.2941](#)].
- [72] S. Choi, S. Jung, and P. Ko, *Implications of LHC data on 125 GeV Higgs-like boson for the Standard Model and its various extensions*, *JHEP* **10** (2013) 225, [[arXiv:1307.3948](#)].
- [73] P. Bechtle, S. Heinemeyer, O. Stål, T. Stefaniak, and G. Weiglein, *Probing the Standard Model with Higgs signal rates from the Tevatron, the LHC and a future ILC*, *JHEP* **11** (2014) 039, [[arXiv:1403.1582](#)].
- [74] J. Bergstrom and S. Riad, *Bayesian Model comparison of Higgs couplings*, *Phys. Rev.* **D91** (2015), no. 7 075008, [[arXiv:1411.4876](#)].
- [75] T. Corbett, O. J. P. Eboli, D. Goncalves, J. Gonzalez-Fraile, T. Plehn, and M. Rauch, *The Higgs Legacy of the LHC Run I*, *JHEP* **08** (2015) 156, [[arXiv:1505.05516](#)].
- [76] **TLEP Design Study Working Group Collaboration**, M. Bicer et al., *First Look at the Physics Case of TLEP*, *JHEP* **01** (2014) 164, [[arXiv:1308.6176](#)].
- [77] T. Barklow, J. Brau, K. Fujii, J. Gao, J. List, N. Walker, and K. Yokoya, *ILC Operating Scenarios*, [arXiv:1506.07830](#).
- [78] K. Fujii et al., *Physics Case for the International Linear Collider*, [arXiv:1506.05992](#).
- [79] **CEPC-SPPC Study Group Collaboration**, *CEPC-SPPC Preliminary Conceptual Design Report*, 2015.
- [80] **CMS Collaboration**, *Projected Performance of an Upgraded CMS Detector at the LHC and HL-LHC: Contribution to the Snowmass Process*, in *Community Summer Study 2013: Snowmass on the Mississippi (CSS2013) Minneapolis, MN, USA, July 29-August 6, 2013*, 2013. [arXiv:1307.7135](#).
- [81] *Projections for measurements of Higgs boson cross sections, branching ratios and coupling parameters with the ATLAS detector at a HL-LHC*, Tech. Rep. ATL-PHYS-PUB-2013-014, CERN, Geneva, Oct, 2013.
- [82] *Prospects for the study of the Higgs boson in the VH(bb) channel at HL-LHC*, Tech. Rep. ATL-PHYS-PUB-2014-011, CERN, Geneva, Jul, 2014.

- [83] *Projections for measurements of Higgs boson signal strengths and coupling parameters with the ATLAS detector at a HL-LHC*, Tech. Rep. ATL-PHYS-PUB-2014-016, CERN, Geneva, Oct, 2014.
- [84] J. Erler, S. Heinemeyer, W. Hollik, G. Weiglein, and P. M. Zerwas, *Physics impact of GigaZ*, *Phys. Lett.* **B486** (2000) 125–133, [[hep-ph/0005024](#)]. [,1389(2000)].
- [85] A. Freitas, K. Hagiwara, S. Heinemeyer, P. Langacker, K. Moenig, M. Tanabashi, and G. W. Wilson, *Exploring Quantum Physics at the ILC*, in *Community Summer Study 2013: Snowmass on the Mississippi (CSS2013) Minneapolis, MN, USA, July 29-August 6, 2013*, 2013. [arXiv:1307.3962](#).
- [86] J. Fan, M. Reece, and L.-T. Wang, *Possible Futures of Electroweak Precision: ILC, FCC-ee, and CEPC*, *JHEP* **09** (2015) 196, [[arXiv:1411.1054](#)].
- [87] P. Azzi, “Progress in FCC-ee experimental studies.” [Talk given at the 2016 FCC Week in Rome](#).
- [88] S. Dawson et al., *Working Group Report: Higgs Boson*, in *Community Summer Study 2013: Snowmass on the Mississippi (CSS2013) Minneapolis, MN, USA, July 29-August 6, 2013*, 2013. [arXiv:1310.8361](#).
- [89] A. Freitas, *Electroweak precision tests in the LHC era and Z-decay form factors at two-loop level*, in *Proceedings, 12th DESY Workshop on Elementary Particle Physics: Loops and Legs in Quantum Field Theory (LL2014)*, 2014. [arXiv:1406.6980](#).
- [90] A. Freitas, *Numerical multi-loop integrals and applications*, [arXiv:1604.00406](#).
- [91] D. M. Asner et al., *Physics at BES-III*, *Int. J. Mod. Phys.* **A24** (2009) S1–794, [[arXiv:0809.1869](#)].
- [92] V. Lubicz, private communication based on [98].
- [93] M. Beneke, *A Quark mass definition adequate for threshold problems*, *Phys. Lett.* **B434** (1998) 115–125, [[hep-ph/9804241](#)].
- [94] A. H. Hoang and T. Teubner, *Top quark pair production close to threshold: Top mass, width and momentum distribution*, *Phys. Rev.* **D60** (1999) 114027, [[hep-ph/9904468](#)].
- [95] M. Beneke, Y. Kiyo, P. Marquard, A. Penin, J. Piclum, and M. Steinhauser, *Next-to-Next-to-Next-to-Leading Order QCD Prediction for the Top Antitop S-Wave Pair Production Cross Section Near Threshold in e^+e^- Annihilation*, *Phys. Rev. Lett.* **115** (2015), no. 19 192001, [[arXiv:1506.06864](#)].
- [96] M. Beneke, A. Maier, J. Piclum, and T. Rauh, *Higgs effects in top anti-top production near threshold in e^+e^- annihilation*, *Nucl. Phys.* **B899** (2015) 180–193, [[arXiv:1506.06865](#)].
- [97] P. Marquard, A. V. Smirnov, V. A. Smirnov, and M. Steinhauser, *Quark Mass Relations to Four-Loop Order in Perturbative QCD*, *Phys. Rev. Lett.* **114** (2015), no. 14 142002, [[arXiv:1502.01030](#)].
- [98] A. Andreazza et al., *What Next: White Paper of the INFN-CSN1*, *Frascati Phys. Ser.* **60** (2015) 1–302.